═══REVIEW COMMONS MANUSCRIPT═══

IMPORTANT:

- Manuscripts submitted to Review Commons are peer reviewed in a journal-agnostic way.
- Upon transfer of the peer reviewed preprint to a journal, the referee reports will be available in full to the handling editor.
- The identity of the referees will NOT be communicated to the authors unless the reviewers choose to sign their report.
- The identity of the referee will be confidentially disclosed to any affiliate journals to which the manuscript is transferred.

GUIDELINES:

- For reviewers: https://www.reviewcommons.org/reviewers
- For authors: https://www.reviewcommons.org/authors

CONTACT:

The Review Commons office can be contacted directly at: office@reviewcommons.org

Evidence for strong cell-scale signalling during planar polarisation in the *Drosophila* wing

Alexandre Carayon[1] and David Strutt[1,2]

[1]School of Biosciences, University of Sheffield, Firth Court, Sheffield, S10 2TN, UK

[2]Corresponding author

*Correspondence: d.strutt@sheffield.ac.uk

Summary

In developing epithelia, cells become planar polarised with asymmetric localisation of the core planar polarity proteins to opposite cell membranes, where they form stable intercellular complexes. Current models differ regarding the signalling mechanisms required for core protein polarisation. Here, we investigate the existence of cell-intrinsic cell-scale signalling *in vivo* in the *Drosophila* pupal wing. We use conditional and restrictive expression tools to spatiotemporally manipulate core protein activity, combined with quantitative measurement of core protein distribution, polarity and stability. Our results provide evidence for a robust cell-scale signal, while arguing against mechanisms that depend on depletion of a limited pool of a core protein or polarised transport of core proteins on microtubules. Furthermore, we show that polarity propagation across a tissue is hard, highlighting the strong intrinsic capacity of individual cells to establish and maintain planar polarity.

Keywords

Development, planar cell polarity (PCP), planar polarity, core pathway, *Drosophila* wing, signalling, microtubules, Frizzled (Fz)

Introduction

Planar polarity (also known as planar cell polarity [PCP]) describes the coordinated polarisation of cells within the tissue plane, and is established by molecular mechanisms that are conserved throughout the animal kingdom (Hale and Strutt, 2015). Examples of planar polarised structures are hair follicles in the skin and cilia on epithelia such as lung, while planar polarity also controls polarised cell movements during gastrulation that promote axis elongation and neural tube closure (Goodrich and Strutt, 2011; Devenport, 2016; Butler and Wallingford, 2017; Davey and Moens, 2017).

Planar polarity has been extensively studied in the *Drosophila* wing, where each cell is planar polarised and produces a distally oriented trichome (Adler, 2002). This depends on activity of the so-called 'core proteins': six proteins that form polarised intercellular complexes at the proximo-distal cell junctions (Goodrich and Strutt, 2011; Devenport, 2014; Harrison et al., 2020). Core protein complexes on the distal cell membrane are composed of the transmembrane protein Frizzled (Fz) and the cytoplasmic proteins Dishevelled (Dsh) and Diego (Dgo), whereas on proximal cell membrane they contain the transmembrane protein Strabismus (Stbm, also known as Van Gogh [Vang]) and the cytoplasmic protein Prickle (Pk), while the transmembrane protein Flamingo (Fmi, also known as Starry Night [Stan]) is localised on both apposing cell membranes (Fig. 1A). This core protein distribution on opposite cell membranes in the hexagonal cells of the wing epithelium results in a characteristic zig-zag core protein localisation pattern (Fig. 1B). Disruption to activity of any single core protein affects this asymmetric pattern of localisation and trichomes no longer point distally (Harrison et al., 2020).

The orientation of planar polarity in the developing *Drosophila* pupal wing is governed by molecular interactions at different scales (Aw and Devenport, 2017; Harrison et al., 2020; Strutt and Strutt, 2021). At the tissue level there are 'global cues', which act to provide an overall direction to planar polarity (Aw and Devenport, 2017). The identities of the global cues in the wing are still unclear, but a key component is mechanical tension from the wing hinge that induces polarised cell flows and cell rearrangements that reorient polarity from a radial to a proximo-distal pattern (Aigouy et al., 2010; Eaton and Jülicher, 2011) (Fig. 1C,C'). The initial polarity bias proposed to be produced by global cues is then thought to be locally amplified by feedback interactions between core protein complexes at the molecular level (Usui et al., 1999; Axelrod, 2001; Strutt, 2001; Brittle et al., 2022). Complexes of the same orientation are suggested to be stabilised by positive feedback interactions whereas complexes of the opposite orientation are destabilised by negative feedback interactions, these events happening at proximal and distal cell membranes, leading to sorting of stable complexes into a uniform orientation (Harrison et al., 2020; Strutt and Strutt, 2021) (Fig. 1A').

Computational studies support the idea that global cues combined with local feedback interactions are sufficient to establish coordinated planar polarity across a tissue (Amonlirdviman et al., 2005; Le Garrec et al., 2006; Fischer et al., 2013). Moreover, they also predict that in the absence of a global cue, local feedback interactions are insufficient to polarise cells. This stands in contrast to *in vivo* studies that show that induction of core pathway activity in the *Drosophila* wing from 16-24h of pupal life can generate *de novo* swirling patterns of planar polarity that appear uncoupled from global cues (Strutt and Strutt, 2002; Strutt and Strutt, 2007). To explain the production of such *de novo* patterns of swirling polarity in the absence of global cues, the existence of 'non-local' cell-

scale signalling has been suggested (Meinhardt, 2007; Burak and Shraiman, 2009; Abley et al., 2013; Shadkhoo and Mani, 2019) (Fig. 1B).

Here, we investigate possible mechanisms by which a cell-scale signal may act during core pathway dependent planar polarisation in the *Drosophila* wing. Based on one suggested scenario (Meinhardt, 2007), we tested a 'depletion' model whereby one or more core proteins is present in limiting amounts for cell for polarisation, thus acting as a non-local inhibitory signal (Fig. 1B). To do this, we set up a system in which we can induce core pathway *de novo* polarisation while varying core pathway gene dosage. We coupled this with use of tagged Fz that acts as a fluorescent timer to discriminate different Fz populations over time. As an alternative possibility, we assessed whether the previously reported transport of core proteins on microtubules (MTs) (Shimada et al., 2006; Harumoto et al., 2010; Matis et al., 2014) could be acting as a cell-scale signal during polarity establishment (Fig. 1B'). Finally, we studied polarity propagation across the tissue caused by induction of a boundary of Fz expression, in an attempt to characterise the properties of the putative cell-scale signal.

Our results argue against roles in mediation of a cell-scale signal for either depletion of a limited pool of a core protein or polarised transport of core proteins on microtubules. Nevertheless, our studies of polarity propagation from boundaries reveal that such propagation is hard to induce even over timescales of hours. This suggests that cells possess a strong intrinsic capacity to polarise and maintain their polarity, implying the existence of a robust cell-scale signal that most likely occurs via a biochemical mechanism such as diffusion of an unidentified inhibitor (Fig. 1B'').

Results

Dynamics of *de novo* planar polarity establishment

To understand mechanisms of core pathway planar polarity establishment, we first followed the process of cell polarisation over time, measuring three parameters: (i) cell polarity orientation (polarity angle), (ii) cell polarity magnitude (polarity strength), and (iii) core protein complex stability. Cell polarity orientation and magnitude were determined using the PCA method in QuantifyPolarity as described previously (Tan et al., 2021). Complex stability was assessed by measuring the dynamics of turnover of the core protein Fz. Fz interacts with Fmi to form the asymmetric backbone of core protein complexes (Strutt and Strutt, 2007; Chen et al., 2008; Strutt and Strutt, 2008; Strutt et al., 2023) and thus its stability is a proxy for overall complex stability. In our experiments Fz is tagged with two distinct fluorescent proteins whose maturation timings are different: sfGFP (superfolder GFP) with a very rapid maturation, showing the total population of Fz, and mKate2 with a slower maturation revealing older (presumed stable) populations of Fz, to form a fluorescent timer (Khmelinskii et al., 2012; Barry et al., 2016; Ressurreicao et al., 2018) (Fig. S1A). The ratio of mKate2/sfGFP is used as a proxy for the proportion of stable Fz.

In wild-type pupal wings, the pattern of core pathway planar polarity depends upon (i) pre-existing polarity established at earlier stages of development, (ii) cell flows and cell re-arrangements that occur during pupal wing morphogenesis (Aigouy et al., 2010). To bypass these events, we studied planar polarisation in a *de novo* polarisation context, generated by induction of Fz expression in a

fz mutant background (Strutt and Strutt, 2002; Strutt and Strutt, 2007) at stages of pupal wing development when cell flows and cell re-arrangements are largely complete.

We used the FLP/FRT recombination system (*FRT-STOP-FRT* cassette excision in the presence of *hsFLP*) (Theodosiou and Xu, 1998) combined with a 1h heat shock (38°C) (Fig. S1B) to induce Fz::mKate2-sfGFP expression under the *Actin5C* promoter in a *fz* mutant background. We initially analysed planar polarity establishment in a flat part of the wing, below longitudinal vein 4 (LV4) and distal to the posterior cross vein (PCV) (Fig. 1C).

To characterise the rate of polarisation and establishment of stable polarity complexes during *de novo* polarity establishment, in the period of pupal wing development prior to emergence of trichomes, we first needed reference measurements for maximally polarised and unpolarised cells. For fully polarised cells, we examined wings that expressed Act-Fz::mKate2-sfGFP throughout development (Fig. 2D). Live imaging, with observation of native sfGFP and mKate2 fluorescence, showed Fz asymmetric localisation at cell junctions in the pupal wing, leading to the specific zig-zag core protein localisation pattern (Fig. 2I'-I''), with a proximo-distal polarity orientation of Fz (Fig. 2I''') and a uniform proximo-distal orientation of trichomes in the adult wing (Fig. 2L), in agreement with previous work (Strutt, 2001). Hence mKate2-sfGFP tagged Fz expressed under the *Actin5C* promoter recapitulates endogenous Fz function.

As an unpolarised condition we used a dsh^1 mutant background, in a *de novo* polarity induction condition for 6h (polarity induction at 22h after prepupa formation [APF] and polarity quantification at 28h APF). We characterised this situation as the lowest polarity condition for our study and defined it as 'non-polarised' cells and low stability core protein complexes (Fig. 2A) consistent with the requirement for Dsh activity for Fz polarisation and stability (Strutt, 2001; Strutt et al., 2011). In this context the specific zig-zag core protein localisation pattern was lost (Fig. 2E'-E'') and Fz polarity as measured by the PCA method was low (Fig. 2E''', 2J).

We then analysed *de novo* polarity induction in a wild-type background, where expression of Fz::mKate2-sfGFP was induced 6h, 8h or 10h prior to observation at 28h APF (Fig.2F-H). Induction of Fz::mKate2 for 6h revealed detectable planar polarity compared to unpolarised cells (*dsh de novo* 6h vs *de novo* 6h; p=0.0007) (Fig. 2J). This polarity increased with induction for 8h and 10h to reach a plateau (Fig. 2J), with a lower peak value than in the control (constitutive Fz::mKate2-sfGFP) condition (*de novo* 10h vs control; p=0.0003). These three *de novo* polarity induction conditions gave swirling patterns of polarity (Fig. 2F''', 2G''', 2H''', 2M), as expected for pathway activation in the absence of proximo-distal global cues (Strutt and Strutt, 2002; Strutt and Strutt, 2007).

Quantification of the stable fraction of Fz (mKate2/sfGFP ratio) revealed that core protein complexes from 6h after polarity induction are more stable than those in unpolarised cells (*dsh de novo* 6h vs *de novo* 6hr; p<0.0001), reaching a similar level of stability as the normal condition 8h after polarity induction (*de novo* 8h vs control; p=0.4411) (Fig. 2K). In summary, our findings reveal that following *de novo* polarity induction in the pupal wing, planar polarity magnitude and complex stability reach a plateau by 8h.

Planar polarity establishment is robust to variation in protein levels of core complex components

After characterisation of *de novo* polarisation induction in our system, we went on to ask whether *de novo* polarisation is sensitive to levels of individual core proteins. Based on theoretical considerations suggesting that cell polarisation depends on a cell-scale inhibitory signal (Meinhardt, 2007), we hypothesised that the levels of one or more core proteins might be limiting for polarisation. This could be due either to levels being limiting for complex formation – thus placing an upper bound on the number of complexes that can form at cell junctions (representing a 'depletion model') (Fig.1B) – or due to a dosage sensitive role in inhibitory interactions that sort proteins within the cell (Fig.1A', 1B'').

We therefore looked at the effects of reducing gene dosage by 50% (i.e. the heterozygous condition) during *de novo* polarisation (6h after induction) and once *de novo* polarisation reaches a plateau (8h after induction), and also compared to polarisation in otherwise normal conditions. We have previously shown that a reduction in gene dosage reduces the amount of protein available to form complexes at cell junctions for Dsh, Dgo, Pk, Fmi and Stbm (Strutt et al., 2016).

We found no significant difference in the degree of polarisation (polarity magnitude) or the stable fraction of Fz in polarity complexes at either 6h (Fig. 3A-H, 3J) or 8h (Fig. S2A-I) after induction, when halving the dosage of *dgo*, *pk*, *stbm* or *fmi*. The exception was for *dsh/+* which showed a weak decrease in Fz stability at 6h after polarity induction (*dsh/+ de novo* 6h vs *de novo* 6h; $p=0.0358$) (Fig. 3J). Wings mutant for *dsh* showed the expected low polarity (*dsh/dsh de novo* 6h vs *de novo* 6h; $p<0.0001$) (Fig. 3H) and low stability (*dsh/dsh de novo* 6h vs *de novo* 6h; $p<0.0001$) (Fig. 3J). Interestingly, we did see an effect of core protein gene dosage on the magnitude of Fz polarity achieved (Fig. 3I), but not on Fz stability (Fig. 3K) under the control condition of constitutive Fz::mKate2-sfGFP expression. Specifically, halving the gene dosage of *dgo*, *pk*, *dsh* and *stbm* resulted in a reduction in polarity magnitude. This is in contrast to previous results when an effect on asymmetry of endogenous Fmi was not detected after halving gene dosages (Strutt et al., 2016). This suggests that polarity of Fz::mKate2-sfGFP expressed constitutively under the *Actin5C* promoter shows enhanced sensitivity to reductions in core protein levels.

We propose that following an initial 'fast' phase of polarisation (up to 8-10h), core pathway polarisation can continue to slowly increase if sufficient protein is available (Fig.2J). In the wild-type condition, levels of Dgo/Pk/Dsh/Stbm may not be limiting compared to levels of Fz-Fmi backbones (Strutt et al., 2016), but in wings continuously expressing Act-Fz::mKate2-sfGFP, Fz-Fmi backbones may be more abundant and Dgo/Pk/Dsh/Stbm levels limit magnitude of polarisation (Fig.3I). Lack of an effect on Fz polarity of halving *fmi* gene dosage further suggests that Fmi itself is not limiting for forming Fz-Fmi backbones that nucleate core protein complexes.

Overall, we conclude that the rates of core pathway *de novo* polarisation (and by extension core pathway polarisation in normal conditions) is extremely robust to variation in protein levels of complex components, particularly during the initial fast phase of polarisation.

Apical microtubules and core proteins are oriented independently of each other

Our results so far fail to provide evidence that the establishment of 'cell-scale' polarity can be explained by depletion of a limiting pool of a core protein, thus restricting the distribution of core protein complexes to only a small region of the cell periphery. They also do not provide strong evidence for core protein dosage-dependent negative interactions that set up cell-scale polarity (Fig.1A', 1B'). We therefore decided to explore another possibility, which is that core protein polarity might depend on polarised microtubule (MT) transport (Fig. 1B'). While loss of core protein function has been reported not to alter proximo-distal MT polarity during stages of pupal wing development when core polarity is normally proximo-distal (Harumoto et al., 2010), this does not rule out the possibility that core proteins help to orient MTs, possibly in parallel to other cues such as cell shape. Such core protein-dependent MT orientation could then amplify core protein polarity through polarised core protein trafficking.

To investigate, we used our system of establishing *de novo* core protein polarity (induction at 22h APF and observation at 28h APF), where core proteins polarise in swirling patterns (Fig.2F,M). To follow core protein and MT polarity and cell shape, we fixed and immunolabelled wings and acquired deconvolved images from a flat region of the wing below longitudinal vein 4. In wild-type wings, cells were elongated (cell eccentricity close to 0.6) (Fig. 4A, Fig. S3B) and were aligned following the proximo-distal axis (cell orientation close to 0°) (Fig. 4D, Fig. S3A). In these cells, both endogenous Stbm protein and MTs were polarised following the same proximo-distal pattern (Fig. 4A''-A'''', 4G, 4J, Fig. S3C, S3E). Without *de novo* polarity induction (non-induced Fz-eYFP in a *fz* mutant background), there was no change in cell orientation and eccentricity compared to the wild-type condition (Fig. 4B, 4E, Fig. S3A, S3B). However, Stbm was located all around the cell perimeter (Fig. 4B'', 4B'''', 4H, Fig. S3C, S3D), while MTs were still aligned following the proximo-distal axis (Fig. 4B''', 4K, Fig. S3E). Induction of *de novo* polarity did not change cell shape and orientation (Fig. 4C, 4F, Fig. S3A, S3B) but induced a swirling core protein polarity with a partial proximo-distal bias in the studied region below vein 4 (Fig. 4C', 4C'''', 4I, Fig. S3C ,S3D), in accordance with the orientation of swirled trichomes in the adult wing (Fig. 2M). The difference in core protein localisation was not associated with a shift in MT orientation; MTs always followed a proximo-distal orientation (Fig. 4C''', 4L, Fig. S3E).

To further explore the relationship between core protein polarisation and MT polarity, we next induced core protein repolarisation along the antero-posterior axis. We created an ectopic Fz boundary along horizontal cell membranes (Fig. 4M) by over-expressing Fz in the *hedgehog* expression domain (posterior compartment) with an inducible UAS/GAL4 system (induction at 22h APF and observation at 28h APF) comprising *hh-GAL4* and a *UAS-FRT-STOP-FRT-fz* transgene in the presence of *hs-FLP*. We then analysed the region of the wing above this area of protein induction, in the region proximal to the anterior cross vein between longitudinal vein 3 and longitudinal vein 4 where we found that there is the strongest and sharpest boundary of Hedgehog expression (see Fig.4O').

Without induction of core protein repolarisation, in this region of the wing endogenous Fz and Stbm were normally localised along medio-lateral cell junctions (Fig. 4N-N''), with a proximo-distal polarity orientation (Fig. 4N'''', 4R-R''', Fig. S3H) as expected. Cells were also oriented along the proximo-distal axis (Fig. 4P-P''', Fig. S3F) with MTs oriented in the same direction (Fig. 4N''', 4T-T''', Fig. S3J).

After induction of core protein repolarisation, a Fz over-expression boundary was observable, defining the boundary 0 with cell row 0 (Fig. 4M, 4O'). This repolarisation resulted in a relocalisation of Stbm along horizontal cell membranes (Fig. 4O''), leading to antero-posterior Stbm repolarisation in rows 0 to 2 (Fig. 4O'''', 4S-S4'', Fig. S3H) and an enrichment of Stbm along boundary 0 due to the Fz over-expression on the opposing boundary (Fig. 4O'', Fig. S3I). Despite the reorientation of polarity revealed by the change in Stbm localisation, MT orientation was unchanged, with a proximo-distal orientation in all cell rows (Fig. 4O''', Fig. 4U-U''', Fig. S3J) and cells oriented along the same axis (Fig. 4Q-Q''', Fig. S3F). We did observe an unexpected slight aspect change towards rounder cells in rows 2 and 3, which are away from the repolarisation boundary (Fig. S3G).

In summary, our results show that core pathway polarity can be established on an orthogonal (antero-posterior) axis with no corresponding change in MT polarity, consistent with MTs and core proteins being oriented independently of each other.

Induced core protein relocalisation on a boundary does not lead to a wave of repolarisation

So far we have presented evidence against cell-scale polarity relying on a 'depletion' mechanism (i.e. not highly sensitive to core protein levels) or a MT transport mechanism. We have also observed that at the cellular level, over a period of 6h an antero-posterior boundary of Fz overexpression can only repolarise core protein localisation for about 2-3 cell rows (Fig.4O, 4S, Fig. S3H). This short range of repolarisation was unexpected, but we note that the same induction regime results in repolarisation of trichomes in the adult wing over about 5-10 rows (Fig.5C), consistent with previous reports (Wu and Mlodzik, 2008). This longer range seen in the adult wing may be due to the longer period of induction.

We hypothesise that the limited ability of a Fz overexpression boundary to repolarise may be due to two factors. First, cells might have a strong intrinsic ability to polarise, while cell-cell coupling of polarity with neighbours might be weak. Once established, polarity is highly robust to the effects of Fz overexpression in neighbouring cells due to relatively weak effects of cell-cell coupling. Second, there might be strong cell-cell coupling of polarity between neighbours. A local perturbation, e.g. over-expression of Fz in a neighbouring row of cells, has little effect on the polarity of neighbouring cells, as their polarity is already strongly coupled to their neighbours in the adjacent region of non-overexpression.

In terms of examining these possibilities, we have already attempted to find conditions that weaken (but do not break) the cell-intrinsic polarisation (Fig. 3) by altering core protein levels, but this was unsuccessful. Moreover, there is no reported way to weaken cell-cell coupling of polarity.

Hence, we decided instead to compare repolarisation in a control condition with constitutive Fz::mKate2-sfGFP expression (where global cues set up proximo-distal polarity), to repolarisation in the *de novo* condition produced by Fz::mKate2-sfGFP induction at 22h APF, where cells are in the process of polarising. Our prediction was that *de novo* polarity would be easy to orient/repolarise by a boundary of Fz overexpression, as cells (and their neighbours) do not have a pre-existing polarity.

We first looked at the polarity of trichomes in the adult wing. In the control condition of constitutive Fz::mKate2-sfGFP expression, proximal to the anterior cross vein between longitudinal vein 3 and longitudinal vein, as expected trichomes are oriented along the proximo-distal axis (Fig. 5A). We found that in this wing region, trichomes also point proximo-distally after *de novo* polarisation induction of Fz::mKate2-sfGFP expression at 22h APF (Fig. 5B). This means we can expect to see repolarisation of this proximo-distal polarity to antero-posterior polarity if we overexpress Fz in the posterior compartment.

Interestingly, induction of repolarisation in both the control and *de novo* conditions resulted in similar degrees of partial trichome repolarisation on the antero-posterior axis (Fig. 5C, 5D). In neither case was trichome repolarisation seen beyond longitudinal vein 3. This result does not fit our prediction of longer-range repolarisation in *de novo*.

We then compared Fz distribution in this region of pupal wings at 28h APF in the same four conditions: control constitutive Fz::mKate2-sfGFP expression, 6h of *de novo* Fz::mKate2-sfGFP polarity establishment, 6h of repolarisation caused by Fz overexpression in the posterior compartment, and 6h of *de novo* polarity with 6h of repolarisation. As we saw in the adult wing, *de novo* polarity was broadly proximo-distal and similar in magnitude to the control polarity establishment in this region (Fig. 5E, 5F, 5I-J'''). In repolarisation in the control condition (Fig. 5G, 5K-K'''), row 0 was strongly repolarised and row 1 polarity was partly repolarised (Fig. 5J vs 5K p=0.0014, 5J' vs 5K' p=0.2945). Hence at the cellular level, polarity propagates poorly from a boundary, although this is sufficient to give a robust adult trichome phenotype (Fig.5C). Repolarisation in *de novo* (Fig.5H, 5L-L''') resembled repolarisation in the control condition (Fig.5G, 5K-K'''), with a strong effect in row 0 (Fig.5L vs 5I p=0.0011), and some repolarisation in row 1 (Fig.5L' vs 5I' p=0.0018). These data indicate that there is no dramatic increase in repolarisation from a boundary in *de novo* as compared to repolarisation in the control condition.

Overall, our results show that it is hard to repolarise from a boundary of Fz overexpression in both control and *de novo* polarity conditions. This suggests that *de novo* polarity is rapidly and robustly established and not easily perturbed by high Fz levels on a neighbouring cell boundary. This is consistent with a strong cell-intrinsic polarisation mechanism, rather than strong cell-cell coupling of polarity.

Cell-intrinsic polarity is robust against local perturbation

Given the different conditions, the similarity of degree of repolarisation in control vs *de novo* conditions was puzzling. We reasoned that there might be differences in these conditions that were masked by simply using measures of overall cell polarity. We therefore carried out a more detailed analysis, measuring levels of proteins on individual cell junctions (Fig. 6A).

In control conditions, as expected, all cells in rows 0 to 3 have similar protein levels on their medio-lateral junctions (Fig. 6B, yellow lines in Fig.6A), and on their horizontal junctions (Fig. 6C, grey lines in Fig.6A), with ~2x higher levels on the medio-lateral junctions, consistent with the observed proximo-distal polarity.

After 6h repolarisation in the control condition, Fz distribution is only significantly altered on the row 0 medio-lateral junction (Fig. 6D) and the boundary 1 horizontal junction between row 0 and row 1

(Fig. 6E). Specifically, Fz is lost from the medio-lateral junctions of cells in row 0 and increased on the horizontal junctions along boundary 1. This is consistent with the changes in cell polarity seen in rows 0 and 1 (Fig. 5G, 5K-K'''), and supports the view that polarity changes only propagate 1-2 rows from a boundary of Fz overexpression.

We then investigated 6h repolarisation under *de novo* conditions. Interestingly, Fz levels along junctions in repolarisation in *de novo* do not exactly mirror those in repolarisation in the control condition. While Fz levels are similarly low on medio-lateral junctions in row 0 (Fig. 6F), they are less high on the horizontal boundary 1 between rows 0 and 1 than in repolarisation in normal condition (Fig. 6G). We questioned whether this difference might be due to the short period of polarisation, but obtained the same result after 10h induction (Fig. S4A-D).

Taken together, our findings reveal that induction of repolarisation from a boundary leads to a new core protein distribution along cell membranes, with relocalisation from medio-lateral junctions to horizontal junctions. However, these core protein relocalisations do not induce polarity rearrangement in neighbouring cells. This failure of repolarisation to propagate beyond 1 row of cells is consistent with the presence of a strong cell-intrinsic polarisation machinery, which is only weakly affected by cell-cell coupling of polarity to neighbours (see Discussion).

Discussion

In this work we have attempted to understand mechanisms of planar polarisation by the core planar polarity pathway. In particular, we sought to characterise the cell-intrinsic polarisation machinery that permits cells in the *Drosophila* pupal wing to *de novo* polarise in the absence of proximo-distal global polarity cues. Through experiments attempting to repolarise tissue from a boundary of Fz overexpression, we provide evidence for strong cell-intrinsic polarisation that is not easily repolarised through cell-cell coupling of polarity. While the nature of the cell-intrinsic polarisation system remains to be fully characterised, our work argues against cell-scale polarity being dependent on either a depletion mechanism that is sensitive to absolute levels of the core proteins, or on reorientation of the apical MT network by core pathway activity.

The establishment of coordinated planar polarity across a tissue is generally agreed to depend on multiple processes acting at different scales (Devenport, 2014; Aw and Devenport, 2017; Butler and Wallingford, 2017; Harrison et al., 2020; Strutt and Strutt, 2021; Brittle et al., 2022). These include global cues at the tissue level working in concert with cell-intrinsic polarisation mechanisms that can amplify polarity either on cell-cell boundaries or at the level of whole cells, and cell-cell coupling of polarity between neighbouring cells (see Fig. 1). An outstanding question is the relative influence of each of these processes on the final polarity pattern.

We used several tools to address this question including: (i) *de novo* induction of core pathway planar polarity, to bypass earlier effects of global cues; (ii) manipulation of core protein gene dosage to test 'depletion' models for cell-scale patterning; (iii) induced repolarisation of planar polarity from a boundary to challenge the effects of cell-intrinsic polarisation mechanisms; and (iv) use of a fluorescent timer to monitor Fz stability simultaneously at multiple cell junctions over time.

Our most surprising result is that repolarisation propagation from a Fz overexpression boundary in the pupal wing is hard and after 6h only extends 1-2 rows at most in both control and *de novo*

conditions (Fig. 5K-L'''). However, we do observe differences between these two conditions. In the control condition (constitutive expression of Fz::mKate2-sfGFP), repolarisation in row 0 occurs via loss of Fz from medio-lateral junctions and accumulation of Fz on the horizontal junction away from the region of overexpression (Fig. 7B). This could be either a redistribution of existing protein via endocytosis and trafficking, or removal and degradation of protein from medio-lateral junctions in parallel with delivery of new protein to the horizontal junction (boundary 1), as previously suggested (Butler and Wallingford, 2017; Warrington et al., 2017). In either case, the results are consistent with a cell-scale signal originating from boundary 0 that promotes Fz removal from medio-lateral junctions and localisation to the opposite horizontal junction. This cell-scale signal could result from ectopic recruitment of Stbm to boundary 0, in combination with Stbm depletion from medio-lateral boundaries. Interestingly, under these repolarisation conditions, the high accumulation of Fz on boundary 1 has only a weak effect on the polarity of the neighbouring cell in row 1. Overall, the repolarisation data in the control condition shows that high Fz in a neighbouring cell can repolarise, but this fails to propagate to the next cell.

In contrast, under *de novo* conditions, a Fz expression boundary results in repolarisation in row 0 that is characterised by low Fz on medio-lateral boundaries, but no strong Fz accumulation on boundary 1 (Fig. 7C). Repolarisation does not significantly propagate into row 1, as was also seen for repolarisation in the normal condition (Fig. 5K, 5L, 6F, 6G). Failure to see high Fz on any of the boundaries in row 0 was unexpected, but may support the presence of a cell-scale signal coming from boundary 0 (due to Stbm sequestration there) preventing Fz from accumulating on medio-lateral junctions. Given the lack of strong Fz polarity in row 0, the failure of polarity to propagate into row 1 is unsurprising, as there is negligible change to Fz levels on boundary 1, so row 1 cells are seemingly in a 'normal' environment.

While we do not clearly understand why propagation from boundaries is hard – particularly in the *de novo* polarisation condition where there is no pre-existing polarity aligned with proximo-distal global cues – our results nevertheless support there being a strong intrinsic polarisation mechanism in cells, that seeks to maintain existing polarity in the face of perturbations.

Our characterisation of the timecourse of *de novo* polarisation at the cellular level (Fig. 2) reveals that establishment of locally coordinated polarity is rapid, with polarity magnitude reaching a plateau at 6h and stability of core protein complexes reaching a plateau by 8h. This suggests an initial 'fast' polarisation phase during which core proteins distribution is set up on opposite cell edges, and then a 'slower' phase in which complexes reach maximum stability. We infer that the fast phase depends on an unknown cell-scale signal, with the slow phase most likely reflecting increased recruitment of core proteins into complexes and stabilisation through formation of biomolecular condensates (Strutt et al., 2016).

While we do not know the nature of the cell-scale signal that underlies the ability of cells to polarise in the absence of a global cue, the ability of both insect and mammalian cells to spontaneously planar polarise with only locally coordinated polarity (Strutt and Strutt, 2002; Strutt and Strutt, 2007; Vladar et al., 2012; Aw et al., 2016), suggests there may be a single universal mechanism. As discussed in previous work (Meinhardt, 2007; Burak and Shraiman, 2009; Abley et al., 2013; Shadkhoo and Mani, 2019), such a signal may be mediated by diffusion of a cytoplasmic protein and might be generated by (for instance) post-translation modification of a core complex component. In this context, it is interesting to note that multiple post-translational modifications of

core proteins have been reported (reviewed in (Harrison et al., 2020)), which represent potential candidate mechanisms.

Acknowledgments

Helen Strutt is thanked for comments on the manuscript, Larra Trinidad, Samantha Warrington and Carl Harrison for useful discussions and the fly room staff for excellent technical support. Natalia Bulgakova and Miguel Ramirez-Morena are thanked for advice on microtubule angle quantification. Imaging was performed in the Wolfson Light Microscopy Facility. The work was funded by a Wellcome Trust Senior Fellowship (210630/Z/18/Z) to DS.

Author contributions

Conceptualisation, A.C. and D.S.; methodology, A.C. and D.S.; formal analysis, A.C.; investigation, A.C.; resources, A.C. and D.S.; writing – original draft, A.C. and D.S.; writing – review & editing, A.C., and D.S.; supervision, D.S.; funding acquisition, D.S.

Conflict of interests

The authors declare that they have no conflict of interest.

Materials and Methods

Resources Table

Antibody	Source	Identifier
Mouse monoclonal anti-α-Tubulin	Sigma	T9026
Rabbit anti-Stbm DS17	Ref (Warrington et al., 2013)	N/A
Rat anti-Stbm DS18	Ref (Strutt and Strutt, 2008)	N/A
Rabbit anti-Fz	Ref (Bastock and Strutt, 2007)	N/A

Fly	Source	Identifier
stbm^{6}	Ref (Wolff and Rubin, 1998)	FlyBase: FBal0062423
dsh^{1}	Ref (Perrimon and Mahowald, 1987)	FlyBase: FBal0003138
dgo^{380}	Ref (Feiguin et al., 2001)	FlyBase: FBal0141190
pk$^{pk\text{-}sple13}$	Ref (Gubb et al., 1999)	N/A
fmi^{E59}	Ref (Usui et al., 1999)	FlyBase: FBal0101421
fz^{P21}	Ref (Jones et al., 1996)	FlyBase:FBal0004937
P[w+, Actin5C-FRT-PolyA-FRT-fz-eYFP]	Ref (Strutt, 2001)	FlyBase: FBtp0017633
ActP-FRT-polyA-FRT-fz-mKate2-sfGFP	Ref (Ressurreicao et al., 2018)	FlyBase: FBal0361851

P[w+, Act>STOP>fz-mKate2-sfGFP]	Ref (Ressurreicao et al., 2018)	FlyBase: FBal0361851
hsFLP[attP2]	Bloomington Drosophila Stock Center	FlyBase: FBti0160508
hsFLP1	Bloomington Drosophila Stock Center	FlyBase: FBti0002044
hsFLP22	Bloomington Drosophila Stock Center	FlyBase: FBti0000785
P[w+, hh-GAL4]	Ref (Tanimoto et al., 2000)	FlyBase: FBal0121962
P[w+, UAS>STOP>FzNL]	This work (on III)	
w^{1118}	Bloomington Drosophila Stock Center	FlyBase: FBal0018186
Chemical	**Source**	**Identifier**
16% paraformaldehyde solution (methanol free)	Agar Scientific	cat#R1026
Triton X-100	VWR	cat#28817.295; CAS: 9002-93-1
Tween-20	VWR	cat#437082Q; CAS: 9005-64-5
Glycerol	VWR	cat#284546F; CAS: 56-81-5
DABCO	Fluka	cat#33480; CAS: 280-57-9
Vectashield	Vector Labs	cat#H-1000-10
Normal Goat Serum	Jackson Labs	cat#005-000-121

Software	
ImageJ 1,54f	https://imagej.nih.gov/ij/ Ref (Schneider et al., 2012)
MatLab R2019b	https://uk.mathworks.com/products/matlab.html
Puncta selection script (MatLab)	Ref (Strutt et al., 2016)
Microtubules orientation script (MatLab)	Ref (Ramirez-Moreno et al., 2023)
GraphPad Prism v9	https://www.graphpad.com
QuantifyPolarity	Ref (Tan et al., 2021)
NIS Elements AR 4.60	Nikon
Tissue Analyzer	https://grr.gred-clermont.fr/labmirouse/software/WebPA/ Ref (Etournay et al., 2016)

Fly genetics and husbandry

Drosophila melanogaster were raised on standard cornmeal/agar/molasses media at 25°C unless otherwise specified. To over-express constructs of interest, the UAS/GAL4 system was used (Brand and Perrimon, 1993), with the *hedgehog-GAL4* (*hh-GAL4*) driver. Prepupa of the appropriate genotype were selected and aged at 25°C as indicated.

For induction and recombination experiments *hsFLP* was used to excise an *FRT-Stop-FRT* cassette to allow expression of *Fz-eYFP (P [w+, Actin>STOP>fz-eYFP])* or *Fz-mKate2-sfGFP*

(*P[w+, Actin>STOP>fz-mKate2-sfGFP]attP2 fz*^{P21}). Heat shocks were performed for two hours at 37°C at 24h APF for microtubule experiments, or for one hour at 37°C at the specified time for other experiments. On the basis of when trichomes subsequently emerge, we observe that development is halted for the period of the heat shock. Pupa were left to age at 25°C before dissecting and were fixed at the same developmental time of 28h APF.

Mutant alleles are described in FlyBase; *stbm*^{6}, *pk-sple*^{13}, *fmi*^{E59}, *fz*^{P21} and *dgo*^{380} are putative null alleles and unable to give rise to functional proteins; *dsh*^{1} gives a strong planar polarity phenotype, but functions normally in Wingless signalling (Axelrod et al., 1998; Boutros et al., 1998). For wings mutant for *dsh*, hemizygous males were analysed.

Full genotypes for each experiment are provided in Supplemental Table 1.

Dissection and immunolabelling of pupal wings

Pupal wings were dissected at 28h APF at room temperature. Briefly, pupae were removed from their pupal case and fixed for 40 min in 4% paraformaldehyde in PBS, or 50 min in 10% paraformaldehyde in PBS for microtubule immunolabelling. Wings were then dissected and the outer cuticle removed, fixed for 10 min in 4% paraformaldehyde in PBS or in 10% paraformaldehyde in PBS for microtubule immunolabelling and were blocked for 1h in PBS containing 0.2% Triton X100 (PTX) and 10% normal goat serum. Primary and secondary antibodies were incubated overnight at 4°C in PTX with 10% normal goat serum, and all washes were in PTX. After immunolabelling, wings were post-fixed in 4% paraformaldehyde in PBS for 10 min. Wings were mounted in 12.5 µl of Vectashield or in 25 µl of PBS containing 10% glycerol and 2.5% DABCO, pH7.5 for microtubule experiments.

Imaging

Pupal wings were oriented along the proximodistal axis using longitudinal vein 4 as the reference and were imaged on a Nikon A1R GaAsP confocal microscope using a 60x NA1.4 apochromatic lens. Imaging of Fz::mKate2-sfGFP was done on live pupae, where a small piece of cuticle was removed from above the pupal wing, and the exposed wing was mounted on strips of double-sided tape in a glass-bottomed dish. Wings were imaged with a pixel size of 80 nm, and the pinhole was set to 1.2 AU. 9 Z-slices separated by 150 nm were imaged, and then the 3 brightest slices around junctions were selected and averaged for each channel in ImageJ.

For microtubule imaging, fixed pupal wings were imaged with a pixel size of 40 nm, and the pinhole was set to 0.4 AU. 19 Z-slices separated by 70 nm were captured. Microtubule images were then deconvolved following the Landweber's method with point scan confocal modality with 10 iterations. The 3 brightest slices around junctions were selected from the deconvolved image stack and averaged for each channel in ImageJ.

Adult wings

Adult wings were dehydrated in isopropanol and mounted in GMM (50% methylsalicylate, 50% Canada Balsam), and incubated overnight on a 60˚C hot plate to clear. Wings were photographed under brightfield illumination on a Leica DMR compound at 20x magnification, with longitudinal vein 4 as the horizontal reference.

Quantification and statistical analysis

Fluorescence detection and quantitation

Membrane masks were generated using Tissue Analyzer (Etournay et al., 2016), and the mean intensity of fluorescence in membranes was measured using an automated MATLAB script (see **Puncta_defined_area** in MATLAB scripts below and (Strutt et al., 2016)). The mean intensity of fluorescence in membranes was determined. Fluorescence on medio-lateral oriented junctions or on horizontal oriented junctions was measured by manual drawing of ROIs in ImageJ. For live imaging, background due to autofluorescence was subtracted, and mean fluorescence intensity was averaged across wings.

The fraction of stable Fz was determined by ratio of mKate2/sfGFP fluorescence intensity. When all genotypes were compared, an ANOVA with Tukey's multiple comparisons test was used, or ANOVAs with Dunnett's or Kruskal-Wallis multiple comparisons tests were used to compare wild-type to mutant backgrounds.

Total Fz intensities were compared with an ANOVA with Holm-Sidak's multiple comparisons test to weigh all conditions or with unpaired t test and Mann-Whitney test to compare fluorescence intensities from two conditions.

Planar polarity

For polarity magnitude and cell orientation analysis QuantifyPolarity software was used (Tan et al., 2021). For Figure 5, custom MATLAB scripts were used to combine polarity magnitude and orientation (see **Combined results for polarity** in MATLAB scripts below), and these were visualised on polar plots (see **Polar plot for polarity** for details in MATLAB scripts below). Statistical tests are described in legend text for each figure. For polarity magnitude comparisons, when all genotypes were compared between them, an ANOVA with Tukey's multiple comparisons test was used, or an ANOVA with Dunnett's multiple comparisons tests was used to compare wild-type to mutant backgrounds, or unpaired Mann-Whitney tests were used to compare with or without repolarisation induction. To compare two conditions for total Fz polarity (orientation and magnitude), Hotelling's T-square tests were used.

Cell and microtubule orientation

Analysis of cell orientation and apical microtubule orientation used custom automated MATLAB image analysis scripts, based on an initial protocol developed by (Gomez et al., 2016; Płochocka et

al., 2021) and improved by (Ramirez-Moreno et al., 2023) (see **Microtubule_orientation** in MATLAB scripts below). When all genotypes were compared between them, an ANOVA with Tukey's multiple comparisons test was used, or unpaired Mann-Whitney tests were used to compare with or without repolarisation induction.

MATLAB scripts

Puncta_defined_area

This is a MATLAB script that measures membrane and puncta intensities on segmented images (Strutt et al., 2016) generated using Tissue Analyzer (Etournay et al., 2016), and was used here to measure total membrane intensity (Mmean).

Microtubule_orientation

The average projections of images with tubulin signals were adjusted so that 0.5% of the pixels with the lowest intensities were set to black and the 0.5% of the pixels with the highest intensities were set to white to normalise the variability in signal between images and increase the contrast. Masks generated using Tissue Analyzer (Etournay et al., 2016) were used to isolate tubulin signals in individual cells. Then, the magnitude of the tubulin signal according to its direction (gradient of the signal) in each cell was calculated by convolving the tubulin signal using two 5 × 5 Sobel operators (Gomez et al., 2016). The resulting distributions of tubulin signals were aligned to their maxima at 0 and averaged for cells with specified eccentricities (0.750 ± 0.025 and 0.800 ± 0.025) to produce average profiles of microtubule angle distributions in cells (Płochocka et al., 2021). At the same time, the unaltered distributions were fitted with the Von Mises distribution and the estimated mean and standard deviation of the fitted curve in each cell. The mean was used as the main direction of the apical microtubule network in this cell and the standard deviation as the measure of the microtubule alignment with each other (Microtubule Standard Deviation, MTSD). Finally, the cell directions were calculated by fitting the pixel coordinates of each cell isolated using masks to an ellipse and obtaining the direction of the long axis of the best-fit ellipse. MTSD was plotted against cell eccentricity for cells with a MTSD <90 excluding cells with unfittable distributions of tubulin signal. This MATLAB code is available at https://github.com/nbul/Cytoskeleton/tree/master/PCP-MT. Angle visualisation and quantification data about directions of cell elongation (the direction of the long axis of the best-fit ellipse), overall directions of microtubule networks and Stbm polarity angle (transferred from QuantifyPolarity) were plotted on image masks produced using Tissue Analyzer (Etournay et al., 2016). Here, the length of plotted lines does not reflect polarity magnitudes or length of elongation but is fixed at half of the average long cell axis. Average cell orientation within each image was used to normalise the Stbm polarity angle, individual cell orientations and microtubule angles for each cell in polar histograms with 9 bins in 0-180° format. Data were mirrored to ease visualisation. Normalised angle data was also used to separate angles into quadrants: between -45°, 45° and between 45°, 135°. The plotting and calculations were performed within the script for the microtubule organisation analysis (https://github.com/nbul/Cytoskeleton/tree/master/PCP-MT).

Combined results for polarity

This is a MATLAB script suitable for combining polarity magnitude and angle results generated by QuantifyPolarity software (see Supplemental Materials).

Polar plot for polarity

This is a MATLAB script suitable for generating polar plots showing polarity magnitude and angle, with results from ‘Combined results for polarity (magnitude + angle)’ MatLab script (see Supplemental Materials).

Figures and Legends

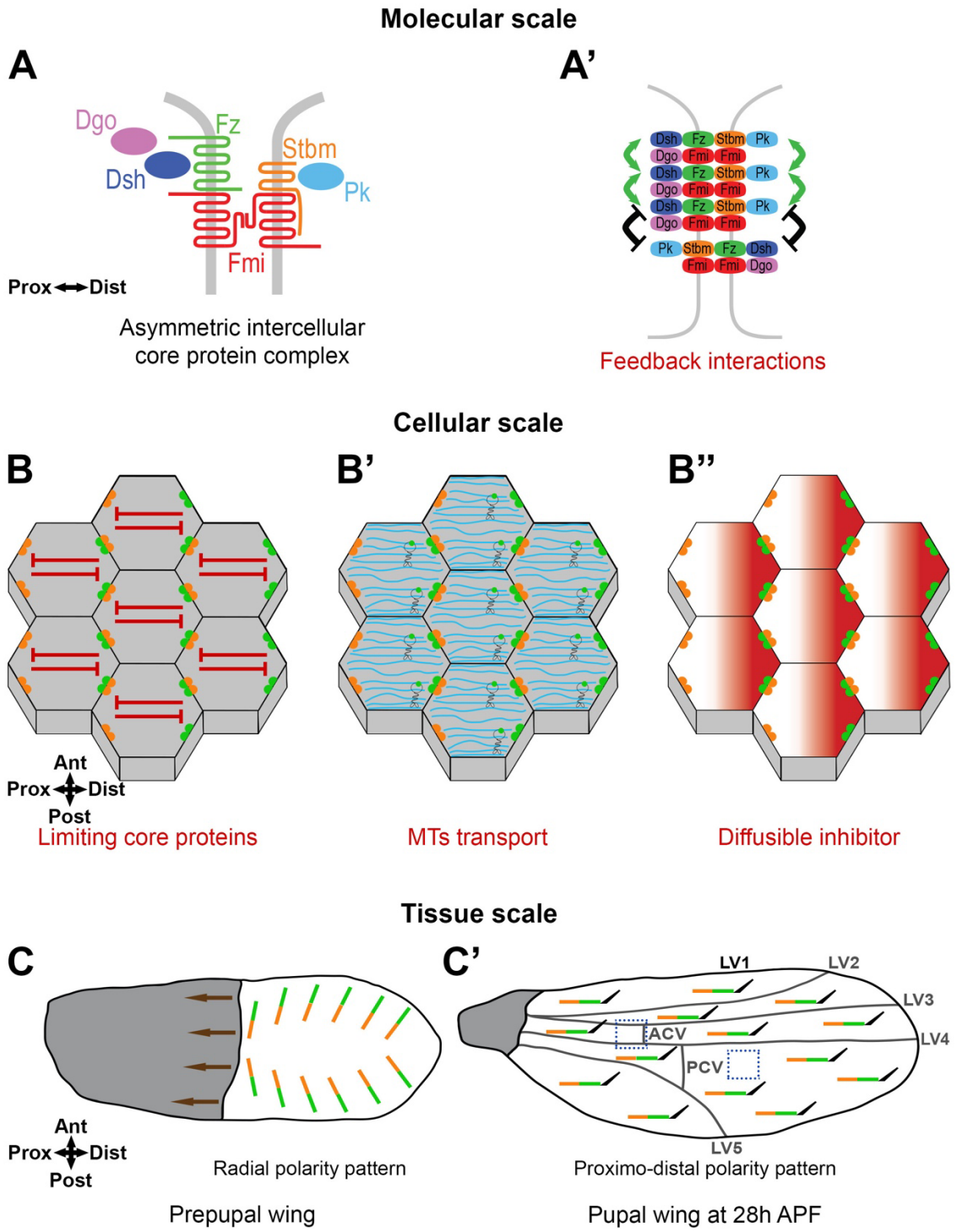

Figure 1. Planar Polarity in the *Drosophila* wing

(A) Core proteins form asymmetric intercellular protein complexes at apicolateral cell membranes mediating intercellular communication. Frizzled (Fz, green) a sevenpass transmembrane protein, and the cytoplasmic proteins Dishevelled (Dsh, dark blue) and Diego (Dgo, magenta) localise to distal cell membranes, while Strabismus (Stbm, orange, also known as Van Gogh [Vang]) a fourpass transmembrane protein and Prickle (Pk, light blue) a cytoplasmic protein, localise to proximal cell membranes. Flamingo (Fmi, red, also known as Starry Night [Stan]) an atypical sevenpass transmembrane cadherin, localises proximally and distally, forming a trans homodimer.

(A') Core protein complexes are thought to interact between themselves through feedback interactions at the molecular level to form stable clusters, with positive interactions stabilising complexes of the same orientation (green arrows) or negative interactions destabilising complexes of opposite orientation (black symbols).

(B-B'') Core protein complexes are segregated to opposite cell membranes generating the specific proximo-distal polarised zig-zag core protein localisation pattern. A potential cell-scale signal would promote this core protein asymmetric distribution. In this study we test several hypotheses to identify this cell-scale signal, such as it being mediated through depletion of a limiting pool of a core protein providing long-range inhibition (red symbols) **(B)**, through oriented MTs transport (MTs in cyan, with motor proteins) **(B')**, or by a biochemical mechanism such as diffusion of an inhibitor **(B'')**.

(C, C') In the 28h pupal wing, core protein polarity (represented by lines with Stbm in orange and Fz in green) and trichome (black hair) orientation is distal **(C')**. It is suggested that this results from radial global cues generating an initial asymmetric bias across the tissue. During earlier polarity establishment in the prepupal wing, hinge contraction (brown arrows) induces cell rearrangements and a redistribution of the core proteins, from the radial polarity pattern in the prepupal wing **(C)** to aligned core protein polarity along the proximo-distal axis of the pupal wing by 28h APF **(C')**.

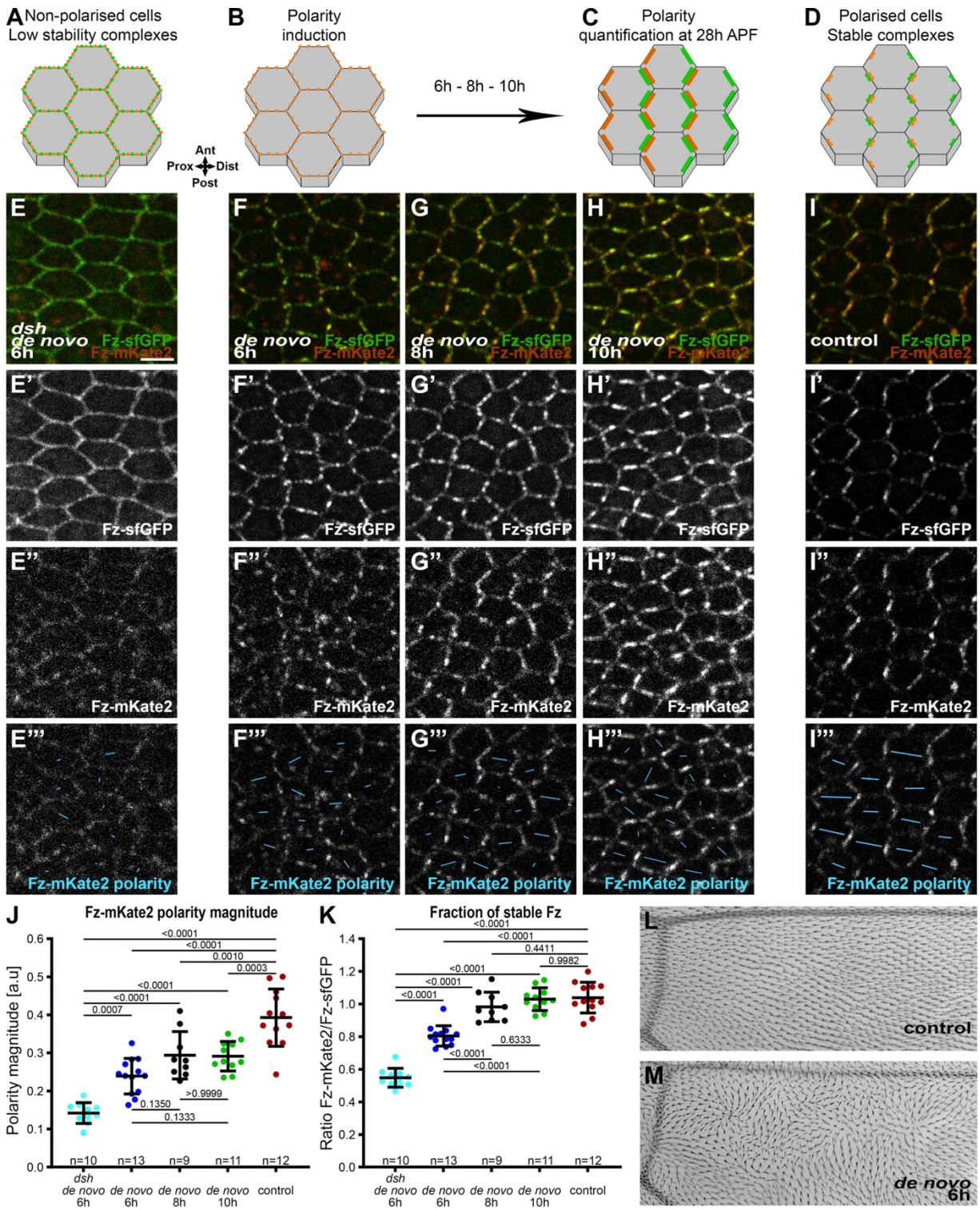

Figure 2. Dynamics of planar polarity establishment

(A-D) Schematics of localisation of core planar polarity pathway protein complexes in cells of the *Drosophila* pupal wing at 28h APF, in non-polarised cells **(A)**, before polarity induction **(B)**, after polarity induction (6h, 8h or 10h) **(C)**, or in the control condition with constitutive expression of Fz::mKate2-sfGFP **(D),** with localisation of Stbm (orange) and Fz (green) at apico-lateral cell junctions indicated. See **Fig. S1B** for induction timings.

(E-I) Live confocal images of 28h APF pupal wing epithelia expressing Fz::mKate2-sfGFP taken below longitudinal vein 4, see **Fig. 1C'** right-hand box. See **Table S1** for full genotypes. Scale bar, 4 µm and the same hereafter. Native fluorescence for sfGFP (green, **E'-I'**) and mKate2 (red, **E''-I''**), with *de novo* condition with 6h induction in a *dsh*^{1} mutant background **(E)**, with *de novo* condition with induction for 6h **(F)**, 8h **(G)**, 10h **(H)** to establish core protein planar polarity; and in the control condition with constitutive expression of Fz::mKate2-sfGFP which gives a normal core protein proximo-distal polarity **(I)**. See **Fig. S1A** for details of Fz tagged to form a fluorescent timer.

(E'''-I''') Cell-by-cell polarity pattern of mKate2 fluorescence in pupal wings expressing Fz::mKate2-sfGFP at 28h APF. The length and orientation of cyan bars denote the polarity magnitude and angle respectively for a given cell**.**

(J, K) Quantified polarity magnitude based on mKate2 fluorescence **(J)** or fraction of stable Fz as determined by ratio of mKate2/sfGFP fluorescence **(K)**, in live pupal wings at 28h APF, in the conditions described in **(E-I)**. Error bars are standard deviation (SD); n, number of wings. ANOVA with Tukey's multiple comparisons test was used to compare all genotypes, p values as indicated.

(L, M) Images of dorsal surface of mounted adult *Drosophila* wings, below longitudinal vein 4. **(L)** Control condition of constitutive Fz::mKate2-sfGFP expression, showing uniform distal orientation of trichomes. **(M)** *de novo* condition after induction at 22h APF, at the equivalent time to the 6h induction when imaging at 28h APF, showing swirled trichome pattern. Proximal is left, and anterior is up.

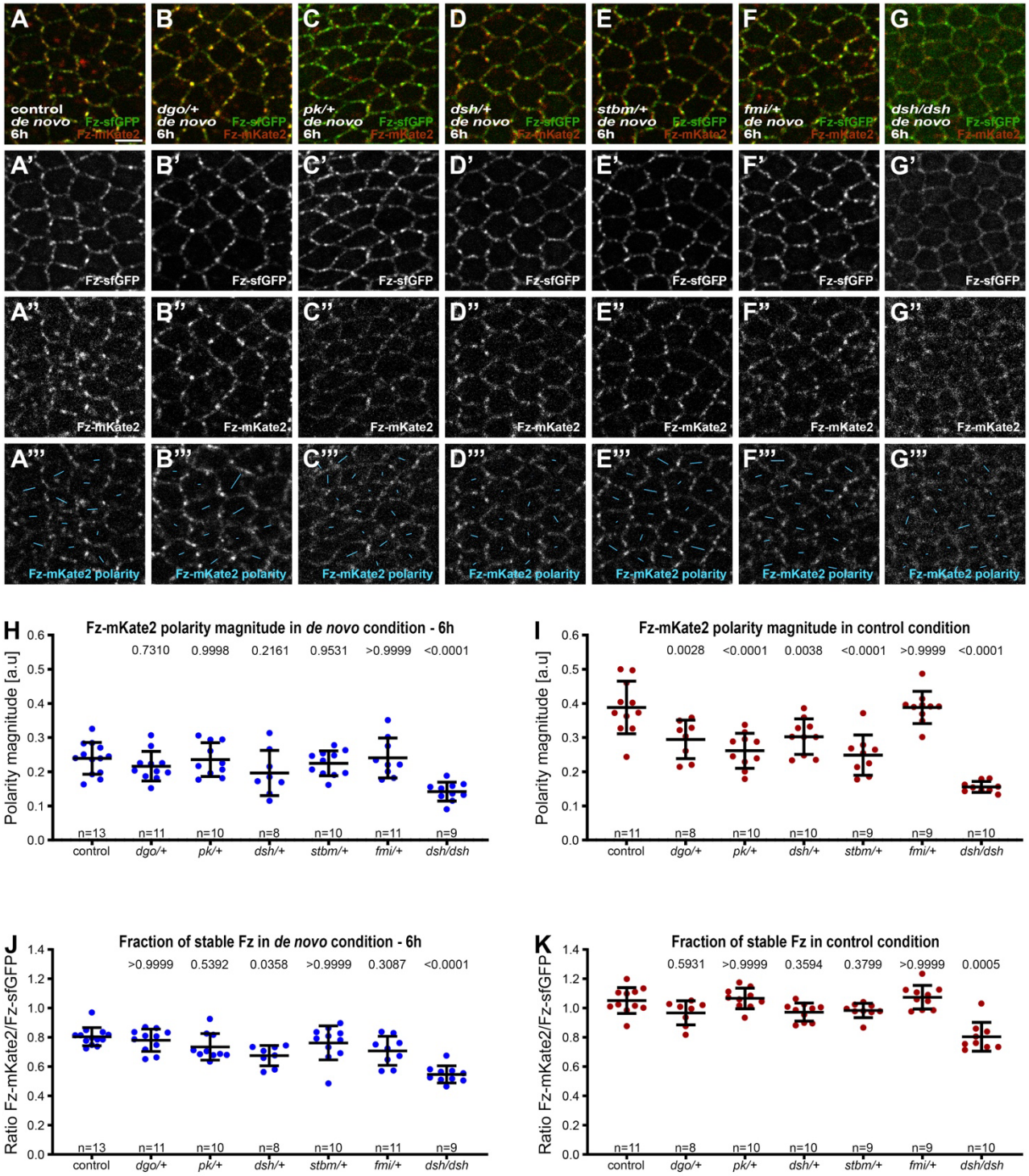

Figure 3. Effect of core protein dosage during *de novo* planar polarity establishment

(A-G) Live confocal images of 28h APF pupal wing epithelia expressing Fz::mKate2-sfGFP, in *de novo* condition taken below longitudinal vein 4. Native fluorescence for sfGFP (green, **A'-G'**) and mKate2 (red, **A''-G''**), with *de novo* condition with 6h induction to establish core protein planar polarity in an otherwise wild-type background **(A)**, heterozygous mutant backgrounds for *dgo* **(B)**, *pk* **(C)**, *dsh*^{1} **(D)**, *stbm* **(E)**, *fmi* **(F)** and hemizygous mutant background for *dsh*^{1} **(G)**. See **Table S1** for the full genotypes. See **Fig. S2** for live confocal images of equivalent 28h APF pupal wing epithelia with constitutive Fz::mKate2-sfGFP expression.

(A'''-G''') Cell-by-cell polarity pattern of mKate2 fluorescence in pupal wings expressing Fz::mKate2-sfGFP at 28h APF. The length and orientation of cyan bars denote the polarity magnitude and angle for a given cell respectively**.**

(H-K) Quantified Fz-mKate2 polarity magnitude based on mKate2 fluorescence **(H, I)** or fraction of stable Fz as determined by ratio of mKate2/sfGFP **(J, K)** in live pupal wings at 28h APF, in the conditions described in **(A-G**). Error bars are SD; n, number of wings. ANOVA with Dunnett's multiple comparisons tests for quantified Fz-mKate2 polarity and ANOVA with Kruskal-Wallis multiple comparisons for fraction of stable Fz, were used to compare wild-type to mutant backgrounds, p values as indicated. See also **Fig. S2**.

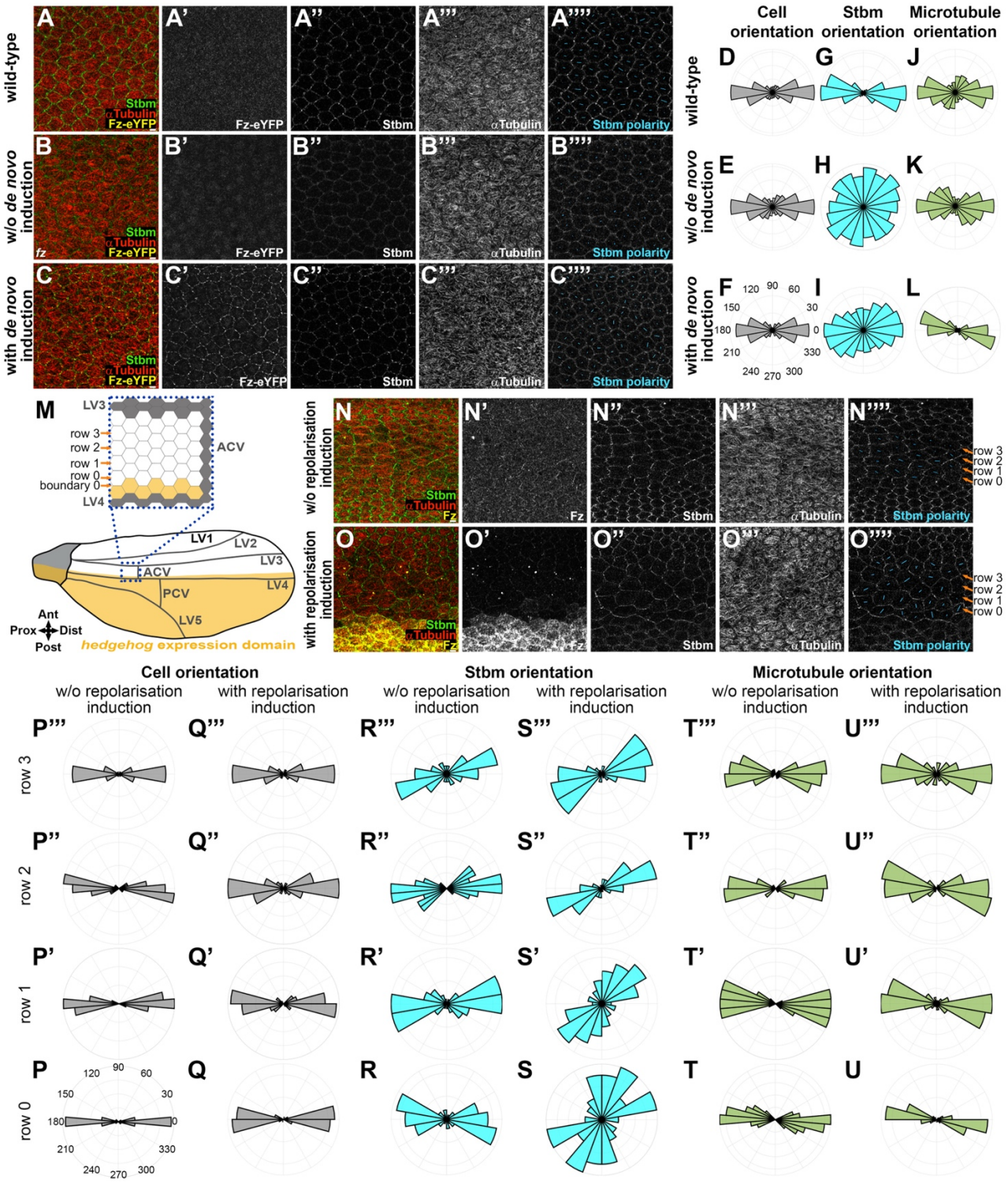

Figure 4. Apical microtubules and core proteins are oriented independently of each other.

(A-C) Apical view of cells with deconvolved confocal images of 28h APF fixed pupal wing epithelia, distal to the posterior cross vein, below longitudinal vein 4, in a wild-type background **(A)**, in *de novo* Fz polarity establishment condition in a *fz* mutant background without polarity induction **(B)** and with polarity induction for 6h **(C)**. Native Fz-eYFP fluorescence (yellow, **A'**, **B'** and **C'**), immunolabelling for Stbm (green, **A''**, **B''** and **C''**) and αTubulin (red, **A'''**, **B'''** and **C'''**). Note there is no Fz-eYFP fluorescence at cell junctions detected in (**A'** and **B'**). Cell-by-cell polarity pattern of pupal wings in respective conditions (**A''''**, **B''''** and **C''''**). The length and orientation of cyan bars

denote the polarity magnitude and angle respectively for a given cell**.** See **Table S1** for the full genotypes. See **Fig. 1C'** for vein locations and imaged wing area.

(D-L) Polar histograms depicting binned cell orientation relative to the horizontal axis **(D-F)**, Stbm polarity orientation **(G-I)** and microtubule orientation **(J-L)** relative to the average cell orientation, in wild-type wings **(D**, **G**, and **J)**, in *de novo* condition without **(E**, **H**, and **K)** or with **(F**, **I**, and **L)** 6h Fz-eYFP polarity induction in fixed pupal wings at 28h APF. n=7-9 wings for each condition. See also **Fig. S3A-E**.

(M) Cartoon of *hedgehog* expression domain (yellow) in the posterior part of the *Drosophila* pupal wing at 28h APF with a zoom in on the proximal region to the anterior cross vein between longitudinal vein 3 and longitudinal 4 (blue dash square). Grey cells are vein cells, white cells are intervein cells and yellow cells are intervein cells with *hedgehog* expression. Boundary 0 is between intervein cells expressing or not expressing *hedgehog* and the first row of intervein cells in contact with cells expressing *hedgehog* across boundary 0 is cell row 0 with anteriorly row 1, 2 and 3.

(N-O) Apical view of cells from deconvolved confocal images of 28h APF fixed pupal wings, in the region proximal to the anterior cross vein between longitudinal vein 3 and longitudinal 4, in an otherwise wild-type background without Fz repolarisation induction **(N)** and with Fz repolarisation induction for 6h **(O)**. For Fz repolarisation conditions, induced Fz is over-expressed in the *hedgehog* expression domain (posterior wing part) with the UAS-GAL4 system **(Fig. 4M)**. Staining as described in **(A-C)**, against Fz **(**yellow, **N'**, **O')**, Stbm **(**green, **N''**, **O'')** and αTubulin **(**red, **N'''**, **O''')**. Cell-by-cell polarity pattern of pupal wings in respective conditions **(N''''**, **O'''')**. The length and orientation of cyan bars denote the polarity magnitude and angle respectively for a given cell**.** See **Table S1** for the full genotypes. See **Fig. 4M** and **Fig. 1C'** for vein locations and imaged wing areas.

(P-U) Polar histograms depicting binned cell orientation relative to the horizontal axis **(P-Q)**, Stbm polarity orientation **(R-S)** and microtubule orientation **(T-U)** relative to the average cell orientation, without **(P**, **R** and **T)** or with **(Q**, **S** and **U)** Fz repolarisation induction for 6h in fixed pupal wings at 28h APF. Cells are grouped in rows relative to their location relative to Fz overexpression (*hedgehog* expression domain) in Fz repolarisation condition or relative to longitudinal vein 4 without Fz repolarisation with row 0 in contact with the *hh-GAL4* overexpression boundary and row 3 furthest away. n=8 wings for both conditions. See also **Fig. S3F-J**.

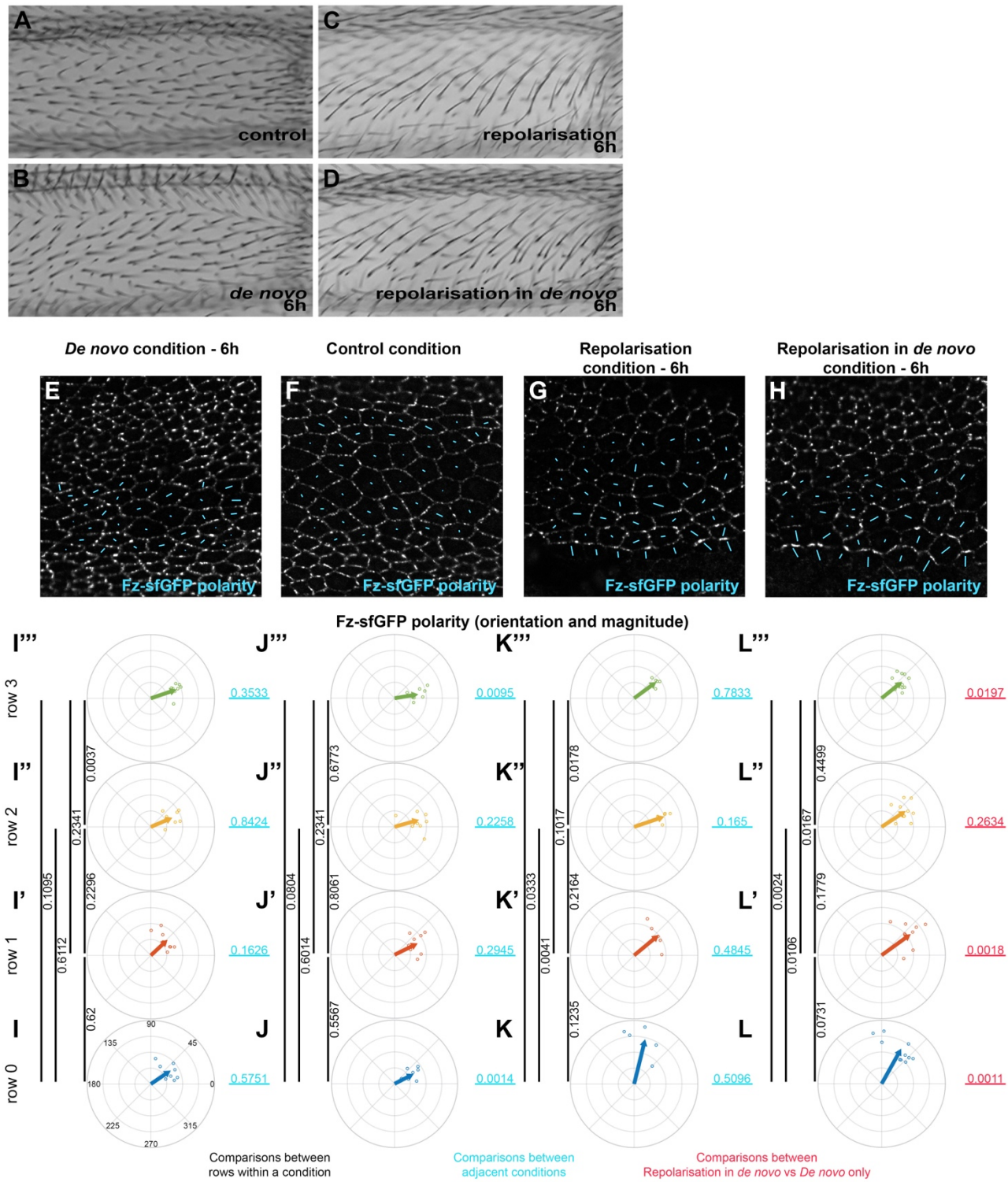

Figure 5. Reorientation of planar polarity from a boundary under control and *de novo* conditions

(A-D) Images of dorsal surface of adult *Drosophila* wings, taken proximal to the anterior cross vein between longitudinal vein 3 and longitudinal vein 4, showing trichome orientation in control condition with constitutive Fz::mKate2-sfGFP expression **(A)**, in *de novo* Fz::mKate2-sfGFP induction condition **(B)**, in repolarisation from the *hh-GAL4* boundary with constitutive Fz::mKate2-sfGFP expression condition **(C)**, and in repolarisation from the *hh-GAL4* boundary under *de novo* Fz::mKate2-sfGFP induction condition **(D)**. Note trichome polarity reorientation in the antero-

posterior direction in both repolarisation conditions. Repolarisation conditions are under UAS-GAL4 control for Fz over-expression in the posterior wing (*hedgehog* expression domain), with induced Fz expression from *UAS-FRT-STOP-FRT-Fz* in the presence of *hsFLP*. See **Fig. 4M** and **Fig. 1C'** for vein locations and imaged wing area. See **Table S1** for the full genotypes.

(E-H) Planar polarity measurement at cellular scale in the region proximal to the anterior cross vein, between longitudinal vein 3 and longitudinal vein 4 in fixed pupal wings at 28h APF. The length and orientation of cyan bars denote the polarity magnitude and angle for a given cell respectively**.** *De novo* condition with 6h induction of Fz::mKate2-sfGFP **(E)**, constitutive expression of Fz::mKate2-sfGFP **(F)**, repolarisation condition with constitutive expression of Fz::mKate2-sfGFP **(G)**, and repolarisation condition with 6h *de novo* induction of Fz::mKate2-sfGFP **(H)**. In repolarisation conditions, induced Fz is over-expressed in the posterior wing, whereas in anterior wing only Fz::mKate2-sfGFP is expressed. In the posterior wing the two Fz populations (over-expressed Fz and Fz::mKate2-sfGFP) compete for the same membrane locations and Fz::mKate2-sfGFP signal is not evident.

(I-L) Circular plots of quantified total Fz (Fz::sfGFP) magnitude and orientation relative to horizontal axis in the region proximal to the anterior cross vein, between longitudinal vein 3 and longitudinal vein 4 at 28h APF in fixed pupal wings. Small dots show polarity angle and magnitude for individual wings, arrows show average polarity and magnitude across all wings. Cells are grouped in rows relative to their location relative to the Fz overexpression domain in Fz repolarisation condition or relative to longitudinal vein 4 without Fz repolarisation, with row 0 in contact with Fz overexpression boundary and row 3 furthest away. **(I-I'''**) *de novo* condition with 6h to establish core protein polarity, **(J-J''')** control condition with constitutive Fz::mKate2-sfGFP expression, **(K-K''')** repolarisation condition for 6h to re-orient core protein polarity, and **(L-L''')** repolarisation under *de novo* condition for 6h induced Fz::mKate2-sfGFP expression**)**; in row 0 **(I**, **J**, **K** and **L)**, in row 1 **(I'**, **J'**, **K'** and **L')**, in row 2 **(I''**, **J''**, **K''** and **L'')** and in row 3 **(I'''**, **J'''**, **K'''** and **L''')**. Vertical black lines associated with p values on right of each column represent comparisons between different rows of the same polarisation condition. Horizontal pale blue lines associated with p values represent comparison between the two adjacent polarisation conditions for the same cell row. On the far right, horizontal red underlined p values represent comparison between Repolarisation in *de novo* condition versus *de novo* condition (far left) for the respective rows of cells. Hotelling's T-square tests were used to compare total Fz polarity (orientation and magnitude).

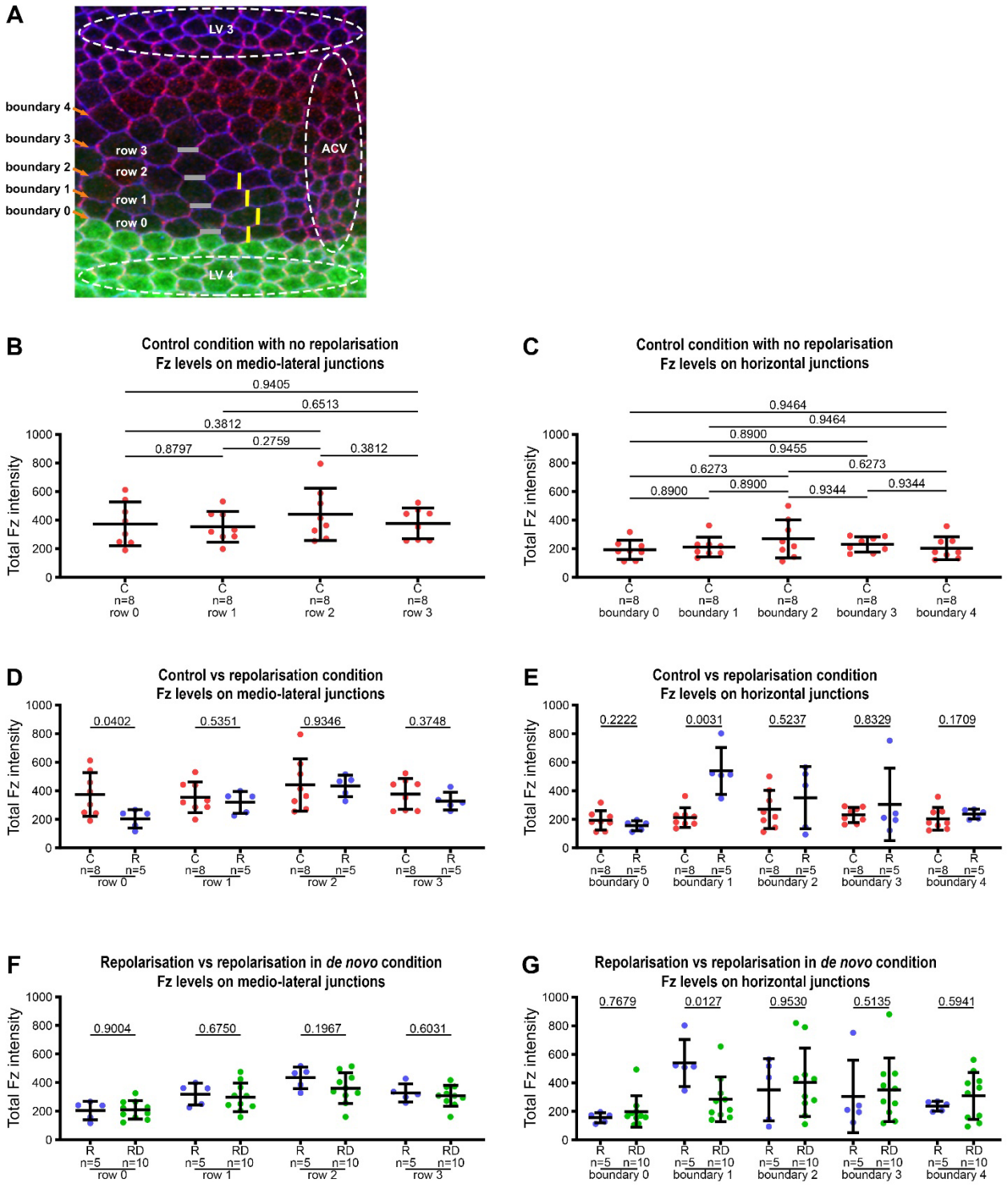

Figure 6. Distribution of Fz along medio-lateral and horizontal junctions in Fz repolarisation and repolarisation under *de novo* conditions.

(A) Explanatory diagram for wing region, cell rows and cell boundaries. Visualisation of the anterior part of the anterior cross vein (ACV) between the longitudinal vein 3 (LV 3) and the longitudinal vein 4 (LV 4) in a fixed pupal wing at 28h APF. Green area indicates the expression domain of the *hh-GAL4* driver used to over-express Fz. E-Cadherin staining is in blue and Stbm staining in magenta. Junctions with horizontal orientation are schematised with grey lines, forming horizontal boundaries with boundary 0 between last row of cells over expressing Fz in LV 4 and the first row

of cells without over expression of Fz in the intervein area (row 0). Medio-lateral junctions are schematised in yellow.

(B-G) Quantitation of Fz intensity in fixed pupal wings at 28h APF, binned by row of cells relative to their location relative to Fz overexpression in Fz repolarisation and Fz repolarisation under *de novo* conditions, or relative to longitudinal vein 4 without Fz repolarisation induction, with row 0 in contact with Fz overexpression boundary and row 3 furthest away. Boundary 0 is the posterior horizontal junction of row 0 in contact with Fz overexpression area and boundary 1 is the anterior horizontal junction shared between cells in row 0 and row 1. See **Table S1** for the full genotypes. Error bars are SD; n, number of wings, p values as indicated.

(B, C) Total Fz intensity in control condition with constitutive Fz::mKate2-sfGFP expression, along medio-lateral junctions **(B)** and along horizontal junctions **(C)**. ANOVA with Holm-Sidak's multiple comparisons test was used to compare all conditions.

(D, E) Comparison of Fz distribution in control condition with constitutive Fz::mKate2-sfGFP expression versus repolarisation condition with 6h induction, along medio-lateral junctions **(D)** and along horizontal junctions **(E)**. Unpaired t test **(D)** and Mann-Whitney test **(E)** were used to compare fluorescence intensities.

(F, G) Comparison of Fz distribution in repolarisation condition versus repolarisation in *de novo* condition with 6h induction, along medio-lateral junctions **(F)** and along horizontal junctions **(G)**. Unpaired t test **(F)** and Mann-Whitney test **(G)** were used to compare fluorescence intensities. See also **Fig. S4**.

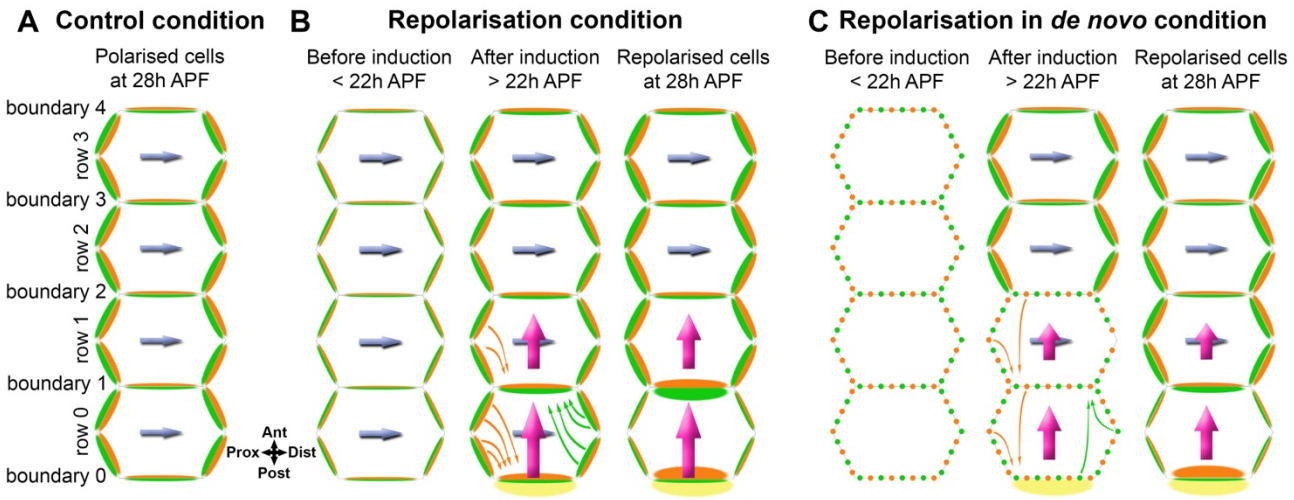

Figure 7. Summary model of polarity propagation confronted with cell-scale polarity.

(A) Core protein polarisation in control (wild-type) conditions at 28h APF. The level of total Fz (green) does not vary significantly on different medio-lateral junctions or on different horizontal junctions. Stbm (orange) levels mirror Fz levels on the same cell junctions. Planar polarity is directed by the integrated effects of an upstream extrinsic global cue and a cell intrinsic cell-scale polarisation system (blue arrow) with a proximo-distal orientation.

(B) Repolarisation of core protein polarity from a boundary. Before repolarisation induction, Fz (green) and Stbm (orange) become polarised following the proximo-distal axis due to the normal extrinsic and intrinsic planar polarity systems (blue arrow). After repolarisation induction by Fz over-expression in the posterior part of the wing, over-expressed Fz (yellow) accumulates on posterior boundary 0. In row 0, Fz is seen to be lost from medio-lateral junctions and to accumulate on the horizontal junction away from the region of overexpression (boundary 1). This could be due to redistribution of existing protein via endocytosis and trafficking (green arrows) or removal and degradation of protein from medio-lateral junctions and net delivery of new protein to horizontal junctions. Stbm redistribution also occurs (orange arrows) with a loss of Stbm from medio-lateral junctions and accumulation on anterior boundary 0. We surmise that Stbm redistribution to boundary 0 is primarily a result of Stbm being sequestered by forming asymmetric complexes with the high levels of over-expressed Fz on the other side of the boundary. In row 1, it is likely that a loss of Stbm located on medio-lateral junctions, and relocation along boundary 1, again occurs via the same potential mechanisms with sequestration into boundary 1 due to accumulation of Fz on the other side of this boundary. We hypothesise that Stbm redistribution to boundaries 0 and 1 results in overall cell repolarisation of rows 0 and 1 through generation of a cell-scale cell intrinsic polarity signal (magenta arrows) that overrides the original cell polarity cues (blue arrows). Notably, repolarisation does not propagate into row 2, presumably due to weak cell-cell coupling of polarity and the strong cell-intrinsic polarity mechanisms in these cells (blue arrows).

(C) Repolarisation of core protein polarity from a boundary in *de novo* conditions. As in repolarisation of core protein polarity in the control conditions, we surmise that Stbm accumulates on boundary 0 in row 0, due to high Fz levels on the other side of the boundary causing Stbm to be sequestered into asymmetric complexes. This could then result in a cell-scale polarity signal (magenta arrows) on the antero-posterior axis that promotes Fz accumulation on boundary 1 in row 0, rather than on mediolateral boundaries. Concurrently, cells in rows 1-3 spontaneously

polarise and adopt a proximo-distal polarity due to the presence of a strong cell intrinsic polarisation system (blue arrows). Weak cell-cell coupling of polarity means that the altered polarity in row 0 does not propagate significantly

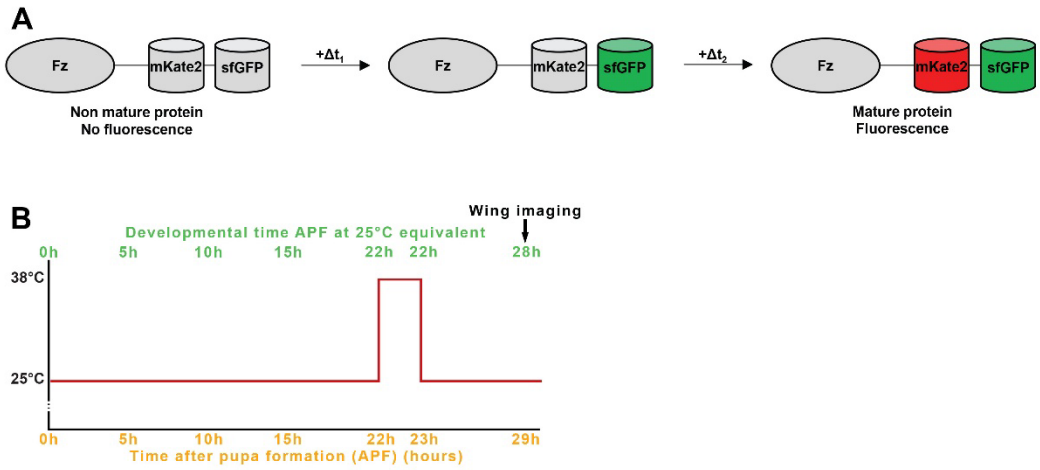

Supplemental Figure 1. Tools for planar polarity characterisation

(A) Schematic illustration of evolution of fluorescent timer fluorescence over time – tandem fusion of mKate2 and sfGFP to Fz.

(B) Scheme of induction of Fz tagged with fluorescent timer expression by heat shock induction, with Fz observation at 28h APF. Here is represented the condition with 6h between tagged Fz expression induction and its observation. With 8h between tagged Fz expression induction and its observation at 28h APF, heat shock is performed at 20h APF and for 10h time difference, at 18h APF. Note wing development is inhibited during the heat-shock period.

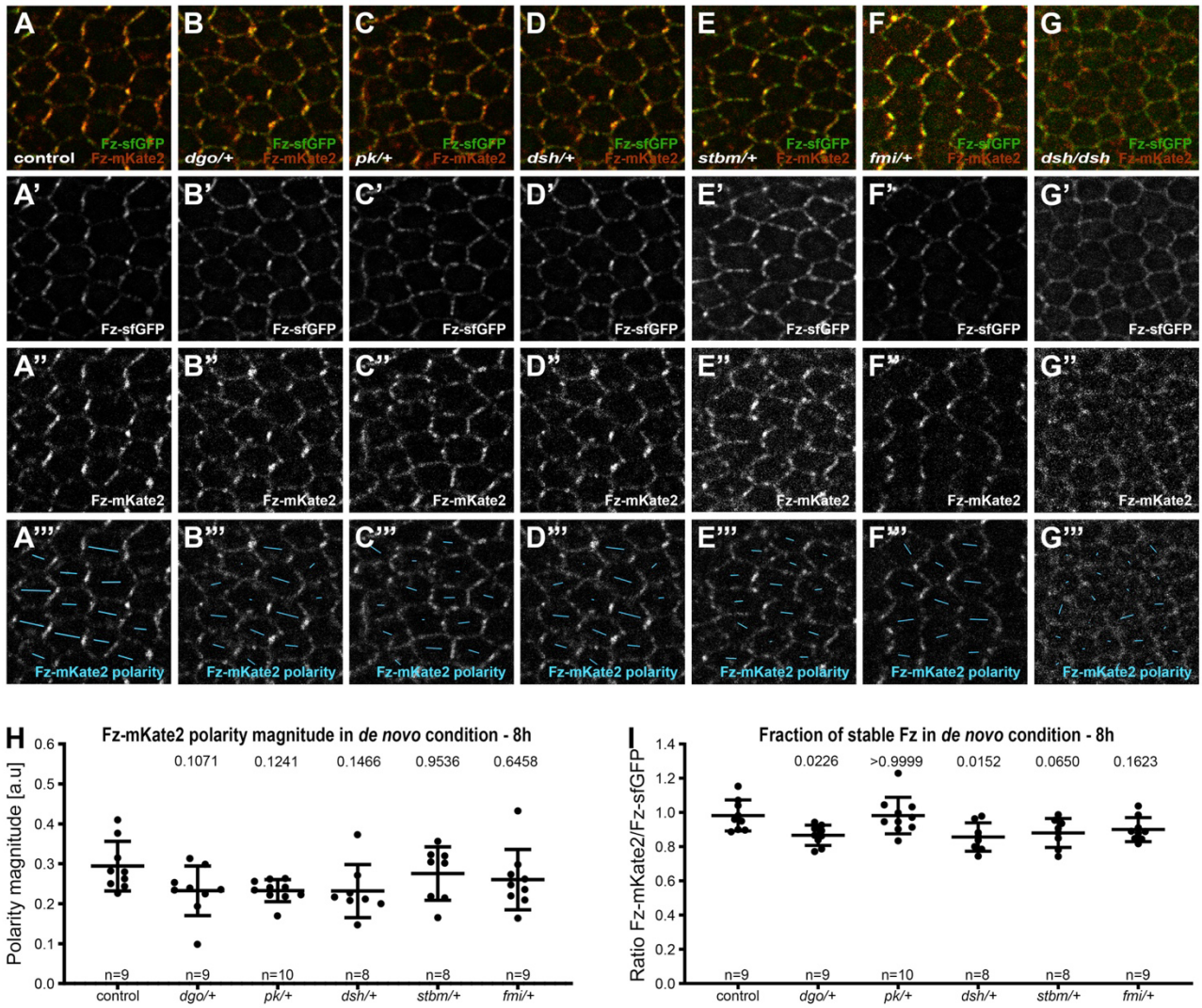

Supplemental Figure 2. Core protein polarity patterns under control conditions and in *de novo* condition with 8h induction to establish planar polarity

(A-G) Live confocal images of 28h APF pupal wing epithelia expressing Fz::mKate2-sfGFP taken below longitudinal vein 4, see **Fig. 1C'**. See **Table S1** for the full genotypes. Native fluorescence for sfGFP **(**green, **A'-G')** and mKate2 **(**red, **A"-G")**, with constitutive expression of Fz::mKate2-sfGFP in an otherwise wild-type background **(A)**, or in heterozygous mutant backgrounds for *dgo* **(B)**, *pk* **(C)**, *dsh*^{1} **(D)**, *stbm* **(E)**, *fmi* **(F)**, and hemizygous mutant background for *dsh*^{1} **(G)**. See **Fig. S1B** for details of Fz tagged with fluorescent timer.

(A'''-G''') Cell-by-cell polarity pattern of mKate2 fluorescence in pupal wings expressing Fz::mKate2-sfGFP at 28h APF. The length and orientation of cyan bars denote the polarity magnitude and angle respectively for a given cell.

(H, I) Quantified polarity magnitude based on mKate2 fluorescence **(H)** or fraction of stable Fz as determined by ratio of mKate2/sfGFP **(I)**, in live pupal wings at 28h APF, in wild-type or core protein heterozygous mutant backgrounds in *de novo* condition with 8h induction of Fz:mKate2-sfGFP to establish core protein planar polarity. Error bars are SD; n, number of wings. ANOVA with Dunnett's multiple comparisons tests were used to compare wild-type to mutant backgrounds, p values as indicated.

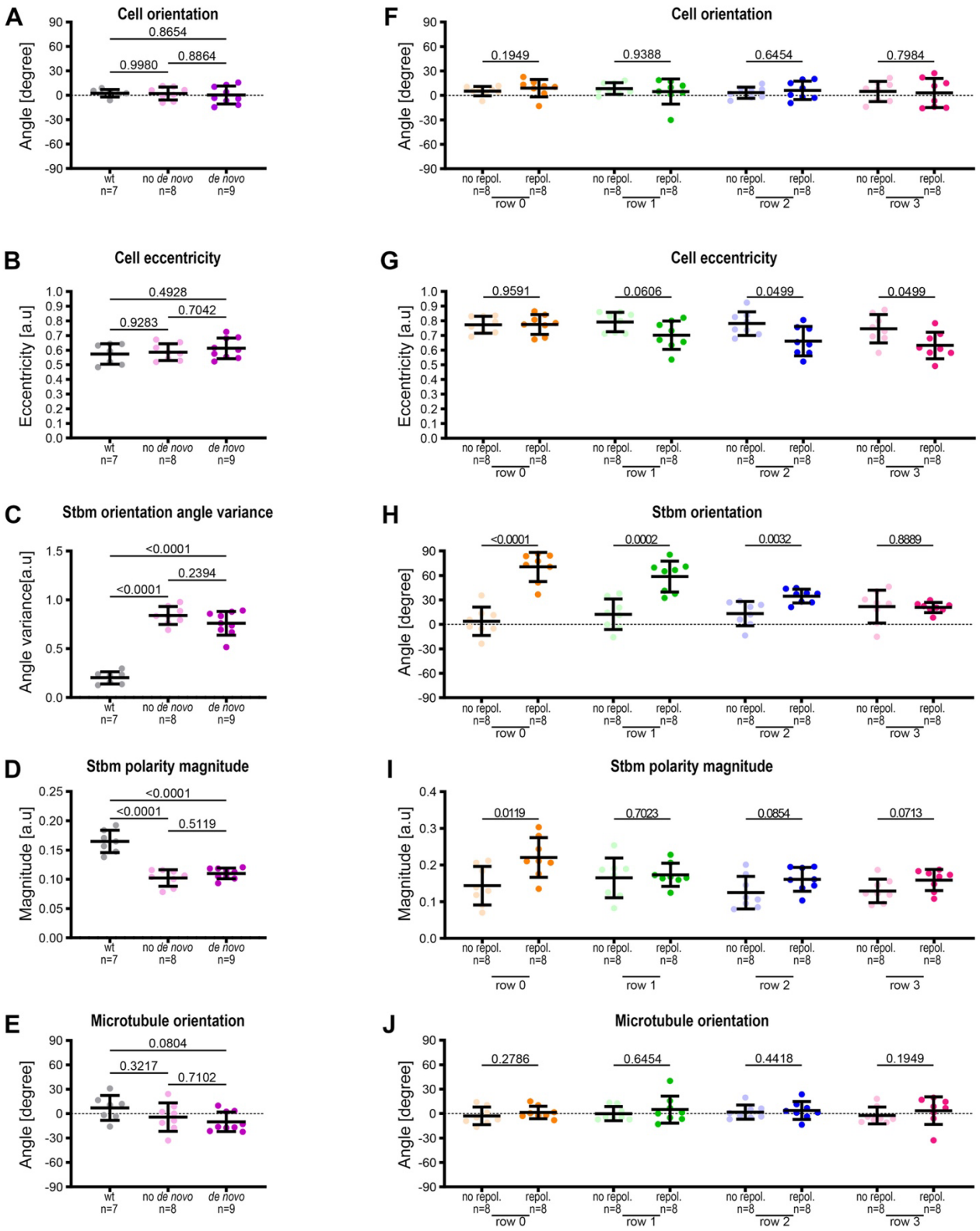

Supplemental Figure 3. Quantification of cell shape, Stbm polarity and microtubule orientation in wild-type and *de novo* and repolarisation conditions at 28h APF.

(A-E) Quantifications from conditions in **Fig. 4A-C** of cell orientation relative to horizontal axis **(A)**, cell eccentricity **(B)**, Stbm orientation angle variance **(C)**, Stbm polarity magnitude **(D)** and microtubule orientation **(E)** relative to the average cell orientation, in wild-type wings, in *de novo*

condition without induction (no *de novo*) or with (*de novo*) Fz-eYFP polarisation induction for 6h, in fixed pupal wings at 28h APF, in the region distal to the posterior cross vein, below longitudinal vein 4. Error bars are SD; n, number of wings. ANOVA with Tukey's multiple comparisons tests were used to compare all genotypes, p values as indicated. See **Table S1** for the full genotypes.

(F-J) Quantifications from conditions in **Fig. 4N-O** of cell orientation relative to horizontal axis **(F)**, cell eccentricity **(G)**, Stbm orientation angle **(H)**, Stbm polarity magnitude **(I)** and microtubule orientation **(J)** relative to the average cell orientation, without (no repol.) or with Fz (repol.) repolarisation induction for 6h, in fixed pupal wings at 28h APF. Cells are grouped in rows relative to their location relative to Fz overexpression in Fz repolarisation condition or relative to longitudinal vein 4 without Fz repolarisation with row 0 in contact with Fz overexpression boundary and row 3 furthest away. Error bars are SD; n, number of wings. Mann-Whitney tests **(F**, **G** and **J)** and Unpaired Mann-Whitney tests **(H**, **I)** were used to compare in each condition with or without Fz repolarisation polarisation induction, p values as indicated. See **Table S1** for the full genotypes.

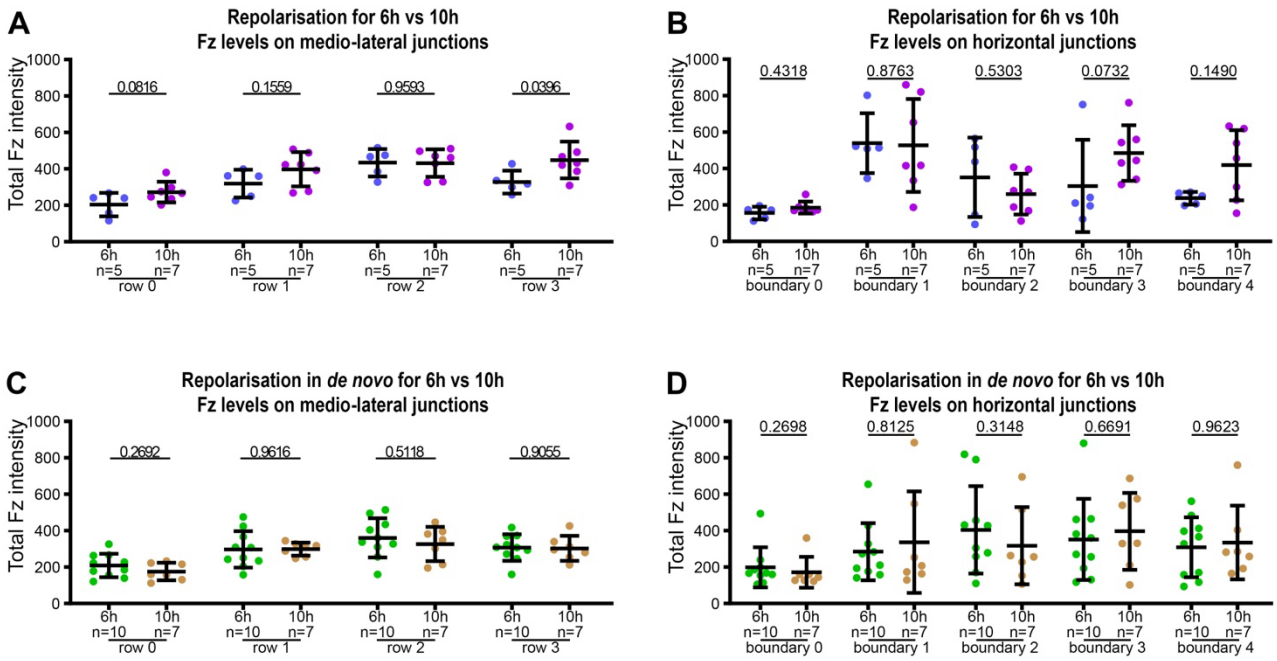

Supplemental Figure 4. Distribution of Fz along medio-lateral and horizontal junctions in repolarisation and repolarisation under 6h and 10h *de novo* induction conditions

Quantitation of Fz intensity in fixed pupal wings at 28h APF, binned by row of cells relative to their location relative to Fz overexpression in Fz repolarisation and Fz repolarisation under *de novo* conditions, with row 0 in contact with Fz overexpression boundary and row 3 furthest away. See **Table S1** for the full genotypes. Error bars are SD; n, number of wings.

(A-B) Comparison of Fz distribution in repolarisation condition with 6h or with 10h to repolarise, along medio-lateral junctions **(A)** and along horizontal junctions **(B)**. Unpaired t test **(A)** and Mann-Whitney test **(B)** were used to compare fluorescence intensity for 6h vs 10h conditions, p values as indicated.

(C-D) Comparison of Fz distribution in repolarisation in *de novo* condition with 6h or 10h induction, along medio-lateral junctions **(C)** and along horizontal junctions **(D)**. Unpaired t test **(C)** and Mann-Whitney test **(D)** were used to compare fluorescence intensity at 6h vs 10h, p values as indicated.

References

Abley, K., P.B. De Reuille, D. Strutt, A. Bangham, P. Prusinkiewicz, A.F. Maree, V.A. Grieneisen, and E. Coen. 2013. An intracellular partitioning-based framework for tissue cell polarity in plants and animals. *Development*. 140:2061-2074. 10.1242/dev.062984.

Adler, P.N. 2002. Planar signaling and morphogenesis in *Drosophila*. *Dev Cell*. 2:525-535. 10.1016/s1534-5807(02)00176-4.

Aigouy, B., R. Farhadifar, D.B. Staple, A. Sagner, J.C. Roper, F. Jülicher, and S. Eaton. 2010. Cell flow reorients the axis of planar polarity in the wing epithelium of *Drosophila*. *Cell*. 142:773-786. 10.1016/j.cell.2010.07.042.

Amonlirdviman, K., N.A. Khare, D.R. Tree, W.S. Chen, J.D. Axelrod, and C.J. Tomlin. 2005. Mathematical modeling of planar cell polarity to understand domineering nonautonomy. *Science*. 307:423-426. 10.1126/science.1105471.

Aw, W.Y., and D. Devenport. 2017. Planar cell polarity: global inputs establishing cellular asymmetry. *Curr Opin Cell Biol*. 44:110-116. 10.1016/j.ceb.2016.08.002.

Aw, W.Y., B.W. Heck, B. Joyce, and D. Devenport. 2016. Transient Tissue-Scale Deformation Coordinates Alignment of Planar Cell Polarity Junctions in the Mammalian Skin. *Curr Biol*. 26:2090-2100. 10.1016/j.cub.2016.06.030.

Axelrod, J.D. 2001. Unipolar membrane association of Dishevelled mediates Frizzled planar cell polarity signaling. *Genes Dev*. 15:1182-1187. 10.1101/gad.890501.

Axelrod, J.D., J.R. Miller, J.M. Shulman, R.T. Moon, and N. Perrimon. 1998. Differential recruitment of Dishevelled provides signaling specificity in the planar cell polarity and Wingless signaling pathways. *Genes Dev*. 12:2610-2622. 10.1101/gad.12.16.2610.

Barry, J.D., E. Dona, D. Gilmour, and W. Huber. 2016. TimerQuant: a modelling approach to tandem fluorescent timer design and data interpretation for measuring protein turnover in embryos. *Development*. 143:174-179. 10.1242/dev.125971.

Bastock, R., and D. Strutt. 2007. The planar polarity pathway promotes coordinated cell migration during *Drosophila* oogenesis. *Development*. 134:3055-3064. 10.1242/dev.010447.

Boutros, M., N. Paricio, D.I. Strutt, and M. Mlodzik. 1998. Dishevelled activates JNK and discriminates between JNK pathways in planar polarity and wingless signaling. *Cell*. 94:109-118. 10.1016/s0092-8674(00)81226-x.

Brand, A.H., and N. Perrimon. 1993. Targeted gene expression as a means of altering cell fates and generating dominant phenotypes. *Development*. 118:401-415. 10.1242/dev.118.2.401.

Brittle, A., S.J. Warrington, H. Strutt, E. Manning, S.E. Tan, and D. Strutt. 2022. Distinct mechanisms of planar polarization by the core and Fat-Dachsous planar polarity pathways in the Drosophila wing. *Cell Rep*. 40:111419. 10.1016/j.celrep.2022.111419.

Burak, Y., and B.I. Shraiman. 2009. Order and stochastic dynamics in *Drosophila* planar cell polarity. *PLoS Comput Biol*. 5:e1000628. 10.1371/journal.pcbi.1000628.

Butler, M.T., and J.B. Wallingford. 2017. Planar cell polarity in development and disease. *Nat Rev Mol Cell Biol*. 18:375-388. 10.1038/nrm.2017.11.

Chen, W.S., D. Antic, M. Matis, C.Y. Logan, M. Povelones, G.A. Anderson, R. Nusse, and J.D. Axelrod. 2008. Asymmetric homotypic interactions of the atypical cadherin Flamingo mediate intercellular polarity signaling. *Cell*. 133:1093-1105. 10.1016/j.cell.2008.04.048.

Davey, C.F., and C.B. Moens. 2017. Planar cell polarity in moving cells: think globally, act locally. *Development*. 144:187-200. 10.1242/dev.122804.

Devenport, D. 2014. The cell biology of planar cell polarity. *J Cell Biol*. 207:171-179. 10.1083/jcb.201408039.

Devenport, D. 2016. Tissue morphodynamics: Translating planar polarity cues into polarized cell behaviors. *Semin Cell Dev Biol*. 55:99-110. 10.1016/j.semcdb.2016.03.012.

Eaton, S., and F. Jülicher. 2011. Cell flow and tissue polarity patterns. *Curr Opin Genet Dev*. 21:747-752. 10.1016/j.gde.2011.08.010.

Etournay, R., M. Merkel, M. Popovic, H. Brandl, N.A. Dye, B. Aigouy, G. Salbreux, S. Eaton, and F. Jülicher. 2016. TissueMiner: A multiscale analysis toolkit to quantify how cellular processes create tissue dynamics. *eLife*. 5. 10.7554/eLife.14334.

Feiguin, F., M. Hannus, M. Mlodzik, and S. Eaton. 2001. The ankyrin repeat protein Diego mediates Frizzled-dependent planar polarization. *Dev Cell*. 1:93-101. 10.1016/s1534-5807(01)00010-7.

Fischer, S., P. Houston, N.A. Monk, and M.R. Owen. 2013. Is a persistent global bias necessary for the establishment of planar cell polarity? *PLoS One*. 8:e60064. 10.1371/journal.pone.0060064.

Gomez, J.M., L. Chumakova, N.A. Bulgakova, and N.H. Brown. 2016. Microtubule organization is determined by the shape of epithelial cells. *Nat Commun*. 7:13172. 10.1038/ncomms13172.

Goodrich, L.V., and D. Strutt. 2011. Principles of planar polarity in animal development. *Development*. 138:1877-1892. 10.1242/dev.054080.

Gubb, D., C. Green, D. Huen, D. Coulson, G. Johnson, D. Tree, S. Collier, and J. Roote. 1999. The balance between isoforms of the Prickle LIM domain protein is critical for planar polarity in *Drosophila* imaginal discs. *Genes Dev*. 13:2315-2327. 10.1101/gad.13.17.2315.

Hale, R., and D. Strutt. 2015. Conservation of planar polarity pathway function across the animal kingdom. *Annu Rev Genet*. 49:529-551. 10.1146/annurev-genet-112414-055224.

Harrison, C., H. Shao, H. Strutt, and D. Strutt. 2020. Molecular mechanisms mediating asymmetric subcellular localisation of the core planar polarity pathway proteins. *Biochem Soc Trans*. 48:1297-1308. 10.1042/BST20190404.

Harumoto, T., M. Ito, Y. Shimada, T.J. Kobayashi, H.R. Ueda, B. Lu, and T. Uemura. 2010. Atypical cadherins Dachsous and Fat control dynamics of noncentrosomal microtubules in planar cell polarity. *Dev Cell*. 19:389-401. 10.1016/j.devcel.2010.08.004.

Jones, K.H., J. Liu, and P.N. Adler. 1996. Molecular analysis of EMS-induced frizzled mutations in *Drosophila melanogaster*. *Genetics*. 142:205-215. 10.1093/genetics/142.1.205.

Khmelinskii, A., P.J. Keller, A. Bartosik, M. Meurer, J.D. Barry, B.R. Mardin, A. Kaufmann, S. Trautmann, M. Wachsmuth, G. Pereira, W. Huber, E. Schiebel, and M. Knop. 2012. Tandem fluorescent protein timers for in vivo analysis of protein dynamics. *Nat Biotechnol*. 30:708-714. 10.1038/nbt.2281.

Le Garrec, J.F., P. Lopez, and M. Kerszberg. 2006. Establishment and maintenance of planar epithelial cell polarity by asymmetric cadherin bridges: a computer model. *Dev Dyn*. 235:235-246. 10.1002/dvdy.20617.

Matis, M., D.A. Russler-Germain, Q. Hu, C.J. Tomlin, and J.D. Axelrod. 2014. Microtubules provide directional information for core PCP function. *eLife*. 3:e02893. 10.7554/eLife.02893.

Meinhardt, H. 2007. Computational modelling of epithelial patterning. *Curr Opin Genet Dev*. 17:272-280. 10.1016/j.gde.2007.05.004.

Perrimon, N., and A.P. Mahowald. 1987. Multiple functions of segment polarity genes in *Drosophila*. *Dev Biol*. 119:587-600. 10.1016/0012-1606(87)90061-3.

Płochocka, A.Z., M. Ramirez Moreno, A.M. Davie, N.A. Bulgakova, and L. Chumakova. 2021. Robustness of the microtubule network self-organization in epithelia. *eLife*. 10. 10.7554/eLife.59529.

Ramirez-Moreno, M., R. Hunton, D. Strutt, and N.A. Bulgakova. 2023. Deciphering the roles of cell shape and Fat and Dachsous planar polarity in arranging the *Drosophila* apical microtubule network through quantitative image analysis. *Mol Biol Cell*. 34:ar55. 10.1091/mbc.E22-09-0442.

Ressurreicao, M., S. Warrington, and D. Strutt. 2018. Rapid disruption of Dishevelled activity uncovers an intercellular role in maintenance of Prickle in core planar polarity protein complexes. *Cell Rep*. 25:1415-1424 e1416. 10.1016/j.celrep.2018.10.039.

Schneider, C.A., W.S. Rasband, and K.W. Eliceiri. 2012. NIH Image to ImageJ: 25 years of image analysis. *Nat Methods*. 9:671-675. 10.1038/nmeth.2089.

Shadkhoo, S., and M. Mani. 2019. The role of intracellular interactions in the collective polarization of tissues and its interplay with cellular geometry. *PLoS Comput Biol*. 15:e1007454. 10.1371/journal.pcbi.1007454.

Shimada, Y., S. Yonemura, H. Ohkura, D. Strutt, and T. Uemura. 2006. Polarized transport of Frizzled along the planar microtubule arrays in *Drosophila* wing epithelium. *Dev Cell*. 10:209-222. 10.1016/j.devcel.2005.11.016.

Strutt, D., and H. Strutt. 2007. Differential activities of the core planar polarity proteins during *Drosophila* wing patterning. *Dev Biol*. 302:181-194. 10.1016/j.ydbio.2006.09.026.

Strutt, D.I. 2001. Asymmetric localization of Frizzled and the establishment of cell polarity in the *Drosophila* wing. *Mol Cell*. 7:367-375. 10.1016/s1097-2765(01)00184-8.

Strutt, H., J. Gamage, and D. Strutt. 2016. Robust asymmetric localization of planar polarity proteins is associated with organization into signalosome-like domains of variable stoichiometry. *Cell Rep*. 17:2660-2671. 10.1016/j.celrep.2016.11.021.

Strutt, H., and D. Strutt. 2002. Nonautonomous planar polarity patterning in *Drosophila*: *dishevelled*-independent functions of *frizzled*. *Dev Cell*. 3:851-863. 10.1016/s1534-5807(02)00363-5.

Strutt, H., and D. Strutt. 2008. Differential stability of flamingo protein complexes underlies the establishment of planar polarity. *Curr Biol*. 18:1555-1564. 10.1016/j.cub.2008.08.063.

Strutt, H., and D. Strutt. 2021. How do the Fat-Dachsous and core planar polarity pathways act together and independently to coordinate polarized cell behaviours? *Open Biol*. 11:200356. 10.1098/rsob.200356.

Strutt, H., S. Warrington, A.C.K. Madathil, T. Langenhan, and D. Strutt. 2023. Molecular symmetry breaking in the Frizzled-dependent planar polarity pathway. *Curr Biol*. 33:5340-5354 e5346. 10.1016/j.cub.2023.10.071.

Strutt, H., S.J. Warrington, and D. Strutt. 2011. Dynamics of core planar polarity protein turnover and stable assembly into discrete membrane subdomains. *Dev Cell*. 20:511-525. 10.1016/j.devcel.2011.03.018.

Tan, S.E., W. Tan, K.H. Fisher, and D. Strutt. 2021. QuantifyPolarity, a new tool-kit for measuring planar polarized protein distributions and cell properties in developing tissues. *Development*. 148:dev198952. 10.1242/dev.198952.

Tanimoto, H., S. Itoh, P. ten Dijke, and T. Tabata. 2000. Hedgehog creates a gradient of DPP activity in *Drosophila* wing imaginal discs. *Mol Cell*. 5:59-71. 10.1016/s1097-2765(00)80403-7.

Theodosiou, N.A., and T. Xu. 1998. Use of FLP/FRT system to study *Drosophila* development. *Methods*. 14:355-365. 10.1006/meth.1998.0591.

Usui, T., Y. Shima, Y. Shimada, S. Hirano, R.W. Burgess, T.L. Schwarz, M. Takeichi, and T. Uemura. 1999. Flamingo, a seven-pass transmembrane cadherin, regulates planar cell polarity under the control of Frizzled. *Cell*. 98:585-595. 10.1016/s0092-8674(00)80046-x.

Vladar, E.K., R.D. Bayly, A.M. Sangoram, M.P. Scott, and J.D. Axelrod. 2012. Microtubules enable the planar cell polarity of airway cilia. *Curr Biol*. 22:2203-2212. 10.1016/j.cub.2012.09.046.

Warrington, S.J., H. Strutt, K.H. Fisher, and D. Strutt. 2017. A dual function for Prickle in regulating Frizzled stability during feedback-dependent amplification of planar polarity. *Curr Biol*. 27:2784-2797. 10.1016/j.cub.2017.08.016.

Warrington, S.J., H. Strutt, and D. Strutt. 2013. The Frizzled-dependent planar polarity pathway locally promotes E-cadherin turnover via recruitment of RhoGEF2. *Development*. 140:1045-1054. 10.1242/dev.088724.

Wolff, T., and G.M. Rubin. 1998. *strabismus*, a novel gene that regulates tissue polarity and cell fate decisions in *Drosophila*. *Development*. 125:1149-1159. 10.1242/dev.125.6.1149.

Wu, J., and M. Mlodzik. 2008. The Frizzled extracellular domain is a ligand for Van Gogh/Stbm during nonautonomous planar cell polarity signaling. *Dev Cell*. 15:462-469. 10.1016/j.devcel.2008.08.004.

Table S1. Genotypes used in each experiment

Figure	Simplified genotype	Complete genotype	Comment
Figure 2	*dsh de novo*	*w dsh^{1} hsFLP22/y;; Act>>fz-mKate2sfGFP, fz^{P21}/fz^{P21}*	male only
	de novo	*w;; hsFLP, fz^{P21}/Act>>fz-mKate2sfGFP, fz^{P21}*	
	control	*w;; Act-fz-mKate2sfGFP, fz^{P21}/fz^{P21}*	
Figure 3	**In *de novo* condition (A-G, H,J)**		
	control	*w;; hsFLP, fz^{P21}/Act>>fz-mKate2sfGFP, fz^{P21}*	
	dgo/+	*w; FRT42 dgo^{380}/+; Act>>fz-mKate2sfGFP, fz^{P21}/ hsFLP, fz^{P21}*	
	pk/+	*w; pk$^{pk\text{-}sple13}$/+; Act>>fzmKate2sfGFP, fz^{P21}/fz^{P21}*	
	dsh/+	*w dsh^{1} hsFLP22/+;; Act>>fz-mKate2sfGFP, fz^{P21}/fz^{P21}*	
	dsh/dsh	*w dsh^{1} hsFLP22/y;; Act>>fz-mKate2sfGFP, fz^{P21}/fz^{P21}*	male only
	stbm/+	*w; stbm^{6}/+; Act>>fz-mKate2sfGFP, fz^{P21}/hsFLP, fz^{P21}*	
	fmi/+	*w; fmi^{E59}/+; Act>>fz-mKate2sfGFP, fz^{P21}(1)/hsFLP, fz^{P21}*	
	In control condition (I,K)		
	control	*w;; Act-fz-mKate2sfGFP, fz^{P21}/fz^{P21}*	
	dgo/+	*w; FRT42 dgo^{380}/+; Act-fzmKate2sfGFP fz^{P21}1.4/ fz^{P21}*	
	pk/+	*w; pk$^{pk\text{-}sple13}$/+; Act-fzmKate2sfGFP, fz^{P21}/fz^{P21}*	
	dsh/+	*w^{1118}dsh^{1}/+;; Act-fz-mKate2sfGFP, fz^{P21}/fz^{P21}*	
	dsh/dsh	*w^{1118} dsh^{1}/y;; Act-fz-mKate2sfGFP, fz^{P21}/fz^{P21}*	male only
	stbm/+	*w; stbm^{6}/+; Act-fz-mKate2sfGFP, fz^{P21}/fz^{P21}*	
	fmi/+	*w; fmi^{E59}/+; Act-fz-mKate2sfGFP, fz^{P21}/fz^{P21}*	
Figure 4	wild-type	*w^{1118}*	with heat shock
	w/o *de novo* induction	*w; Act>>fz-eYFP$^{4.1}$/+; fz^{P21}/fz^{P21}*	with heat shock
	with *de novo* induction	*w hsFLP/+; Act>>fz-eYFP$^{4.1}$/+; fz^{P21},FRT80/fz^{P21}*	with heat shock
	w/o repolarisation induction	*w;; hh-Gal4/UAS>>Fz [NL]*	with heat shock
	with repolarisation induction	*w hsFLP/+;; hh-Gal4/UAS>>Fz [NL]*	with heat shock
Figure 5	control	*y w hsFLP/+;; UAS>>fz[NL], Act-fz-mKate2sfGFP, fz^{P21}/hh-Gal4, fz^{P21}*	without heat shock
	de novo	*w;; hsFLP, fz^{P21}/Act>>fz-mKate2sfGFP, fz^{P21}*	with heat shock
	repolarisation	*y w hsFLP/+;; UAS>>fz[NL], Act-fz-mKate2sfGFP, fz^{P21}/hh-Gal4, fz^{P21}*	with heat shock
	repolarisation in *de novo*	*y w hsFLP/+;; UAS>>fz[NL], Act>>fz-mKate2sfGFP, fz^{P21}IH/hh-Gal4, fz^{P21}*	with heat shock
Figure 6	control	*y w hsFLP/+;; UAS>>fz[NL], Act-fz-mKate2sfGFP, fz^{P21}/hh-Gal4, fz^{P21}*	without heat shock
	repolarisation	*y w hsFLP/+;; UAS>>fz[NL], Act-fz-mKate2sfGFP, fzP21/hh-Gal4, fz^{P21}*	with heat shock
	repolarisation in *de novo*	*y w hsFLP/+;; UAS>>fz[NL], Act>>fz-mKate2sfGFP, fzP21IH/hh-Gal4, fz^{P21}*	with heat shock
Fig.S2	**In control condition (A-G)**		
	control	*w;; Act-fz-mKate2sfGFP, fz^{P21}/fz^{P21}*	
	dgo/+	*w; FRT42 dgo^{380}/+; Act-fzmKate2sfGFP fz^{P21}1.4/ fz^{P21}*	
	pk/+	*w; pk$^{pk\text{-}sple13}$/+; Act-fzmKate2sfGFP, fz^{P21}/fz^{P21}*	

	dsh/+	*$w^{1118}dsh^{1}$/+;; Act-fz-mKate2sfGFP, fz^{P21}/fz^{P21}*	
	dsh/dsh	*w^{1118} dsh^{1}/y;; Act-fz-mKate2sfGFP, fz^{P21}/fz^{P21}*	male only
	stbm/+	*w; $stbm^{6}$/+; Act-fz-mKate2sfGFP, fz^{P21}/fz^{P21}*	
	fmi/+	*w; fmi^{E59}/+; Act-fz-mKate2sfGFP, fz^{P21}/fz^{P21}*	
	In de novo condition (H,I)		
	control	*w;; hsFLP, fz^{P21}/Act>>fz-mKate2sfGFP, fz^{P21}*	
	dgo/+	*w; FRT42 dgo^{380}/+; Act>>fz-mKate2sfGFP, fz^{P21}1.4/ hsFLP, fz^{P21}*	
	pk/+	*w; $pk^{pk\text{-}sple13}$cn/+; Act>>fzmKate2sfGFP, fz^{P21}/fz^{P21}*	
	dsh/+	*w dsh^{1} hsFLP22(7)/+;; Act>>fz-mKate2sfGFP, fz^{P21}/fz^{P21}*	
	stbm/+	*w; $stbm^{6}$/+; Act>>fz-mKate2sfGFP, fz^{P21}/hsFLP, fz^{P21}*	
	fmi/+	*w; fmi^{E59}/+; Act>>fz-mKate2sfGFP, fz^{P21}(1)/hsFLP, fz^{P21}*	
Fig.S3	wt	*w^{1118}*	with heat shock
	no *de novo*	*w; Act>>fz-eYFP$^{4.1}$/+; fz^{P21}/fz^{P21}*	with heat shock
	de novo	*w hsFLP/+; Act>>fz-eYFP$^{4.1}$/+; fz^{P21},FRT80/fz^{P21}*	with heat shock
	no repol.	*w;; hh-Gal4/UAS>>fz[NL]*	with heat shock
	repol.	*w hsFLP/+;; hh-Gal4/UAS>>fz[NL]*	with heat shock
Fig.S4	repolarisation	*y w hsFLP/+;; UAS>>fz[NL], Act-fz-mKate2sfGFP, fz^{P21}/hh-Gal4, fz^{P21}*	with heat shock
	repolarisation in *de novo*	*y w hsFLP/+;; UAS>>fz[NL], Act>>fz-mKate2sfGFP, fz^{P21}/hh-Gal4, fz^{P21}*	with heat shock

Table S2A. Normality test for repolarisation from a boundary data (see Fig. 5I-L)

Shapiro-Wilk normality test p-value	**Control condition**	***De novo* condition**	**Repolarisation condition**	**Repolarisation in *de novo* condition**
row 0	0.6254	0.2762	0.3410	0.0208
row 1	0.3963	0.6336	0.0005	0.0657
row 2	0.0673	0.2762	0.0015	0.5750
row 3	0.0737	0.2762	0.0075	0.3361

Normality polarity angle combined with polarity magnitude
Before performing Hotelling's T2 test, confirm that data supports normality
(using multivariate Shapiro-Wilks test) - p-value > 0,05 supports normality

Hotelling's T-square test is robust to violations of assumptions of multivariate normality

from https://online,stat,psu,edu/stat505/lesson/7/7,2/7,2,6

Table S2B. Hotelling's T-square test for repolarisation from a boundary data (see Fig. 5I-L)

Hotelling's T-square test p-value	**row 0**	**row 1**	**row 2**	**row 3**
***De novo* vs control condit**	0.5751	0.1626	0.8424	0.3533
Control vs repolarisation condition	0.0014	0.2945	0.2258	0.0095
Repolarisation vs repolarisation in *de novo* condition	0.5096	0.4845	0.1650	0.7833
Repolarisation in *de novo vs* de *novo* condition	0.0011	0.0018	0.2634	0.0197

Hotelling's T-square test p-value	**Control condition**	***De novo* condition**	**Repolarisation condition**	**Repolarisation in *de novo* condition**
row 0 vs row 1	0.5567	0.6200	0.1235	0.0731
row 1 vs row 2	0.8061	0.2296	0.2164	0.1779
row 2 vs row3	0.6773	0.0037	0.0178	0.4499
row 0 vs row 2	0.6014	0.6112	0.0041	0.0106
row 1 vs row 3	0.2341	0.2341	0.1017	0.0167
row 0 vs row 3	0.0804	0.1095	0.0333	0.0024

Supplemental Materials – Analysis script 1

Combined results for polarity (magnitude + angle)

This is a MATLAB script suitable for combining polarity magnitude and angle results generated by QuantifyPolarity software.

This script is designed to analyse files for 4 conditions (row1, row2, row3 and row4). In order to use it you have to strictly follow the following architecture:

- Create a folder, for row1 analysis, named 'Analysed_sfGFP_row1' containing analysed data from QuantifyPolarity software which own 'Result' subfolder. Do the same thing for row2 up to row4.
- Run the script and choose the appropriate folder location when prompted.

The script redistributes polarity angles in a range between -45° and 135° from −90° and +90° for each analysed cells per wing for all conditions. For each wing of the same condition (for example 'row1'), those reoriented angles are averaged as polarity magnitude and added in a new saved .csv file 'Analysed_sfGFP_row1' in column 'Average_Reoriented_Angle_Polarity_deg'. For each condition, the mean of polarity magnitude and angle is calculated and added in a saved new .csv file 'Average_Reoriented_Angle_Polarity_row1'.

```
clc
 clear all
 close all
 warning off
```

```
%% To locate file

currdir = pwd;
addpath(pwd);
filedir = uigetdir();
cd(filedir);


rootdir=filedir;


myfolder = [filedir];% location of the folder with files to convert
```

```
%% Get a list of all csv files in the current folder, or subfolders of it.


filePattern = fullfile(myfolder, '\Analysed*', '\*', '\Result', 'PCA_Cell-by-
Cell_Polarity.csv'); % Change to whatever pattern you need.




fds = fileDatastore(filePattern, 'ReadFcn', @importdata);
```

```
fullFileNames = fds.Files;


numFiles = length(fullFileNames);


% Loop over all files reading them in and plotting them.


for k = 1 : numFiles


% fprintf('Now reading file %s\n', fullFileNames{k});


% Now have code to read in the data using whatever function you want


    A  = readtable(fullFileNames{k});
    A.Properties.VariableNames = ["Cell Identity", "PCA Magnitude", "PCA
Angle(degrees)"];
```

```
%% To redistribute polarity angles in a range between -45° and 135° from –90° and
90° for each analysed cells per wing



B = xlsread(fullFileNames{k},'C:C'); % to transform data in column C
x = B;
y = numel(x);


for i = 1:y
    if x(i)<=90  && x(i)>=90
    elseif x(i)<-45
         z(i)=180+x(i);
    elseif x(i)>-45
         z(i)=x(i);
         end

end


    B=array2table(z(:)); % this converts the results into a table format.
    B.Properties.VariableNames = ["Reoriented PCA Angle(degrees)"];


    C = [A, B];
   writetable(C, fullFileNames{k});
clearvars z;
end
```

```
%% Get a list of all csv files in the current folder, or subfolders of it.


filePattern = fullfile(myfolder,'\Analysed*', '\*', '\Result', 'PCA_Cell-by-
Cell_Polarity.csv'); % Change to whatever pattern you need.


filePattern1 = fullfile(myfolder,'\Analysed*', '\*', '\Result');
fds1 = fileDatastore(filePattern1, 'ReadFcn', @importdata);
fullFileNames1 = fds1.Files;


filePattern2 = fullfile(myfolder,'\Analysed*', '\*', '\Result',
'*PCA_Average_Polarity_Magnitude.csv');


fds = fileDatastore(filePattern, 'ReadFcn', @importdata);


fullFileNames = fds.Files;


fds2 = fileDatastore(filePattern2, 'ReadFcn', @importdata);


fullFileNames2 = fds2.Files;


filePattern3 = fullfile(myfolder,'\Analysed*', '\*', '\Result',
'*PCA_Average_Polarity_Magnitude.csv');
fds3 = fileDatastore(filePattern3, 'ReadFcn', @importdata);
fullFileName3 = fds3.Files;




numFiles = length(fullFileNames);



% Loop over all files reading them in and plotting them.


 for k = 1 : numFiles



    A  = readtable(fullFileNames{k});
```

```
    D = readtable(fullFileNames2{k});



%% To get Average of Polarity angle


B = xlsread(fullFileNames{k},'D:D'); %to transform data in column D


data = B;
x = data;
y = numel(x);




             ang_rad  = deg2rad (x);
             x(x == 0) = NaN;
             data_avg = sum(exp(1i*ang_rad(:)));


            % obtain mean by
            mu = angle(data_avg);
            Average_Polarity_Angle_mean_degrees = rad2deg(mu);


            T = array2table(Average_Polarity_Angle_mean_degrees);
            T.Properties.VariableNames(1:1) =
{'Average_Reoriented_Angle_Polarity(deg)'};


Reoriented_PCA_Average_Polarity_Magnitude = [D T]; % combine
'*_PCA_Average_Polarity_Magnitude' with 'Average_Reoriented_Angle_Polarity'
R = Reoriented_PCA_Average_Polarity_Magnitude;




writetable(R,['Reoriented_PCA_Average_Polarity_Magnitude_',num2str(k),'.xlsx']);
```

```
filePattern4 = fullfile(myfolder, '*.xlsx' ); % Change to whatever pattern you
need.
```

```
%
fileDatastore(location,"ReadFcn",@customreader,"FileExtensions",[".exts",".extx"]).


fds4 = fileDatastore(filePattern4, 'ReadFcn', @importdata);


fullFileNames4 = fds4.Files;









numFiles4 = length(fullFileNames4);



% Loop over all files reading them in and plotting them.



 Folder1 = filePattern1; % asks user for a folder
FilePattern = fullfile(Folder1,'*PCA_Average_Polarity_Magnitude*.csv');
Files1 = dir(FilePattern); % puts files into struct array
for n = 1 : 1 : numFiles4
% Get input filename.
    fullFileName = fullfile(Files1.folder, Files1.name);
%     fprintf('Reading "%s".\n', fullFileName);
    % Call your function to read the .dta file and put it into a table variable.
    properFolder2 = myfolder;
    properFilePattern = [myfolder, '\Reoriented_PCA_Average_Polarity_Magnitude_*'];
    properFiles2 = dir(properFilePattern); % puts files into struct array
    properfullFileName = fullfile(properFiles2.folder, properFiles2.name);

    properthisTable = readtable(properfullFileName);
    thisTable = readtable(properfullFileName);
     R_Trace_data{n} = properthisTable;
    % Get output filename.  It's the same except the extension is txt instead of
dta.



    [filepath,name,ext] = fileparts(fullFileName);


     outputFullFileName = [name '.xlsx'];
```

```
% Get input filename.
    fullFileName5 = fullfile(Files1(k).folder, Files1(k).name);

    outputFullFileName = strrep(fullFileName5, '.xlsx', '.csv');


   writetable(R_Trace_data{n}, outputFullFileName);




delete (myfolder, '*Reoriented*');
     end



 end


delete (myfolder, '*Reoriented*');
```

```
%% Analysis row1, to combine wings results in 1 .csv file


rootdir=[filedir,'\Analysed_sfGFP_row1']; %  'Analysed_sfGFP_row1' is the name used
there to put
myFiles = (fullfile(rootdir,'\Analysed_sfGFP_row1', '\*', '\Result',
'*PCA_Average_Polarity_Magnitude.csv'));   % Get list of .csv files to combine
(with this script, the file with PCA_Average_Polarity_Magnitude results)
ds = tabularTextDatastore((fullfile(rootdir, '\*', '\Result',
'*PCA_Average_Polarity_Magnitude.csv')));
T = readall(ds);









% To name the combined csv file as the folder containing it
file = rootdir;
[filepath,name,ext] = fileparts(file);
filename1 = name;
writetable(T, filename1); % to write the table T, here .txt


% To name the .csv as the folder containing it
dinfo = dir('*.txt');
filenames = {dinfo.name};
for K = 1 : length(filenames)
  thisfile = filenames{K};
  [basedir, basename, ~] = fileparts(thisfile);
  newfile = fullfile(basedir, [basename '.csv']);
```

```
  writetable(T, newfile)
end


  delete('*.txt');
```

```
%% Analysis row2, to combine wings results in 1 .csv file


rootdir=[filedir,'\Analysed_sfGFP_row2'];
myFiles = (fullfile(rootdir,'\Analysed_sfGFP_row2', '\*', '\Result',
'*PCA_Average_Polarity_Magnitude.csv'));   % Get list of .csv files to combine
(with this script, the file with PCA_Average_Polarity_Magnitude results)
ds = tabularTextDatastore((fullfile(rootdir, '\*', '\Result',
'*PCA_Average_Polarity_Magnitude.csv')));
T = readall(ds);









% To name the combined csv file as the folder containing it
file = rootdir;
[filepath,name,ext] = fileparts(file);
filename1 = name;
writetable(T, filename1); % to write the table T, here .txt


% To name the .csv as the folder containing it
dinfo = dir('*.txt');
filenames = {dinfo.name};
for K = 1 : length(filenames)
  thisfile = filenames{K};
  [basedir, basename, ~] = fileparts(thisfile);
  newfile = fullfile(basedir, [basename '.csv']);
  writetable(T, newfile)
end


  delete('*.txt');
```

```
%% Analysis row3, to combine wings results in 1 .csv file


  rootdir=[filedir,'\Analysed_sfGFP_row3'];
```

```
myFiles = (fullfile(rootdir,'\Analysed_sfGFP_row3', '\*', '\Result',
'*PCA_Average_Polarity_Magnitude.csv'));   % Get list of .csv files to combine
(with this script, the file with PCA_Average_Polarity_Magnitude results)
ds = tabularTextDatastore((fullfile(rootdir, '\*', '\Result',
'*PCA_Average_Polarity_Magnitude.csv')));
T = readall(ds);









% To name the combined csv file as the folder containing it
file = rootdir;
[filepath,name,ext] = fileparts(file);
filename1 = name;
writetable(T, filename1); % to write the table T, here .txt


% To name the .csv as the folder containing it
dinfo = dir('*.txt');
filenames = {dinfo.name};
for K = 1 : length(filenames)
  thisfile = filenames{K};
  [basedir, basename, ~] = fileparts(thisfile);
  newfile = fullfile(basedir, [basename '.csv']);
  writetable(T, newfile)
end


  delete('*.txt');
```

```
%% Analysis row4, to combine wings results in 1 .csv file


rootdir=[filedir,'\Analysed_sfGFP_row4'];
myFiles = (fullfile(rootdir,'\Analysed_sfGFP_row4', '\*', '\Result',
'*PCA_Average_Polarity_Magnitude.csv'));   % Get list of .csv files to combine
(with this script, the file with PCA_Average_Polarity_Magnitude results)
ds = tabularTextDatastore((fullfile(rootdir, '\*', '\Result',
'*PCA_Average_Polarity_Magnitude.csv')));
T = readall(ds);









% To name the combined csv file as the folder containing it
file = rootdir;
```

```
[filepath,name,ext] = fileparts(file);
filename1 = name;
writetable(T, filename1); % to write the table T, here .txt


% To name the .csv as the folder containing it
dinfo = dir('*.txt');
filenames = {dinfo.name};
for K = 1 : length(filenames)
  thisfile = filenames{K};
  [basedir, basename, ~] = fileparts(thisfile);
  newfile = fullfile(basedir, [basename '.csv']);
  writetable(T, newfile)
end


  delete('*.txt');
```

```
%% To get averaged data by row


myfolder = [filedir];% location of the folder with files to convert


  %% Get a list of all csv files in the current folder, or subfolders of it.


filePattern = fullfile(myfolder, 'Analysed_sfGFP_row*.csv'); % Change to whatever
pattern you need.


filePattern1 = fullfile(myfolder);


filePattern2 = fullfile(myfolder, 'Analysed_sfGFP_row*.csv');


fds = fileDatastore(filePattern, 'ReadFcn', @importdata);


fullFileNames = fds.Files;


fds2 = fileDatastore(filePattern2, 'ReadFcn', @importdata);


fullFileNames2 = fds2.Files;



numFiles = length(fullFileNames);
```

```
% Loop over all files reading them in and plotting them.

 for k = 1 : numFiles



    A  = readtable(fullFileNames{k});

    D = readtable(fullFileNames2{k});



% To get Average of Polarity angle

B = xlsread(fullFileNames{k},'J:J'); %to transform data in column D

data = B;
x = data;
y = numel(x);

             ang_rad  = deg2rad (x);
             x(x == 0) = NaN;
             data_avg = sum(exp(1i*ang_rad(:)));

            % obtain mean by
            mu = angle(data_avg);
            Average_Polarity_Angle_mean_degrees = rad2deg(mu);



            data_mean  = Average_Polarity_Angle_mean_degrees;
            T = array2table(Average_Polarity_Angle_mean_degrees);
            T.Properties.VariableNames(1:1) =
{'Average_Reoriented_Angle_Polarity_deg'};



str = 'Average_Reoriented_Angle_Polarity';
t = 0;
    t = t + 1;


% To get Average Polarity Magnitude
```

```
E = xlsread(fullFileNames{k},'E:E'); %to transform data in column D


data = E;
x = data;
y = numel(x);


            % obtain mean by
            mu_Polarity = mean (data);
            Average_Polarity_Magnitude = mu_Polarity;




            data_mean  = Average_Polarity_Magnitude;
            P = array2table(Average_Polarity_Magnitude);
            P.Properties.VariableNames(1:1) = {'Average_Polarity_Magnitude'};





str = 'Average_Polarity_Magnitude';
t = 0;


    t = t + 1;


    R = [P, T];


    writetable(R,['Average_Reoriented_Angle_Polarity_row',num2str(k),'.csv']);
```

```
% clc
% clear variables
% close all


fprintf(1, 'Et voilà!');
```

Supplemental Materials – Analysis script 2

Polar plot for polarity (magnitude + angle)

This is a MATLAB script suitable for generating polar plot showing polarity magnitude and angle, with results from 'Combined results for polarity (magnitude + angle)' MatLab script.

This script draw polar plot, with polarity magnitude and angle for each wing (empty circles) for one condition (example with row1) with results from 'Analysed_sfGFP_row1' that is file with averaged data per wing. It is added average polarity magnitude and angle for all wings from the same condition (filled circle) with results coming from 'Average_Reoriented_Angle_Polarity_row1)

- Open the script, choose which condition to analyse by changing files name ''Analysed_sfGFP_row1.csv'' and ''Average_Reoriented_Angle_Polarity_row1.csv'' by proper files name.
- Run the script.
- Figure is saved in .pdf file with customised title.
- Circle colour and polar plot figure format can by change in the script following instructions.

```
clc
 clear all
 close all
 warning off
```

```
%% To add individual wing results to the graph

myDir = uigetdir ();
cd(myDir);
myFiles = dir(fullfile(myDir, 'Analysed_sfGFP_row1.csv')); %to choose which row to
analyse


L = length (myFiles);


for i=1:L
    data{i} = readtable (myFiles(i).name);
    T = data{i};

    PCAMagnitude {i} = T. AveragePolarityMagnitude;
    PolarityAngle {i} = T. Average_Reoriented_Angle_Polarity_deg_;

    ang_deg  = [PolarityAngle {i}]; %  angles
    ang_rad {i} = ang_deg {i} *pi/180; % convert degrees to radians for polarplot
    magnitude {i} = PCAMagnitude {i}; %  magnitude to plot

    C = ang_rad {i};
    D = magnitude {i};
```

```
%     newcolors = {'#0072BD', '#D95319', '#EDB120', '#77AC30', '#7E2F8E',
'#FF0000','#FFFF00', '#FF00FF', '#C0C0C0', '#00FFFF' }; % to choose colors
(https://htmlcolorcodes.com/fr/), here set up for 12 different colors, if more than
12 samples, add more colors
    newcolors = {'#0072BD'}; % to choose the color
    colororder(newcolors)
%     s.SizeData = 10;


    hs {i} = polarscatter (C, D, 5);
     hold on


end




Legend=cell(i,1);
 for iter=1:i
     Legend{iter}=strcat('row#', num2str(iter));



 end
 hold on


%% To add averaged results from all wings to the graph

 myFiles = dir(fullfile(myDir, 'Average_Reoriented_Angle_Polarity_row1.csv')); %to
choose which row to analyse




L = length (myFiles);


for i=1:L
    data{i} = readtable (myFiles(i).name);
    T = data{i};

    PCAMagnitude_Avg {i} = T. Average_Polarity_Magnitude;
    PolarityAngle_Avg {i} = T. Average_Reoriented_Angle_Polarity_deg;

    ang_deg_Avg  = [PolarityAngle_Avg {i}]; %  angles
    ang_rad_Avg {i} = ang_deg_Avg {i} *pi/180; % convert degrees to radians for
polarplot
    magnitude_Avg {i} = PCAMagnitude_Avg {i}; %  magnitude to plot

    G = ang_rad_Avg {i};
    H = magnitude_Avg {i};
```

```
 % newcolors = {'#D95319', '#EDB120', '#EDB120', '#77AC30', '#0072BD', '#D95319',
'#EDB120', '#77AC30', '#7E2F8E', '#FF0000','#FFFF00', '#FF00FF', '#C0C0C0',
'#00FFFF' }; % to choose colors (https://htmlcolorcodes.com/fr/), here set up for
12 different colors, if more than 12 samples, add more colors
    newcolors = {'#0072BD'}; % to choose the color
    colororder(newcolors)




    hs {i} = polarscatter (G, H, "filled");
    hold on


end




Legend=cell(i,1);
 for iter=1:i
     Legend{iter}=strcat('row#', num2str(iter));



 end




%legend(Legend) %to add legend



rlim([0 0.4]); % x-axis scale


thetaticks(0:45:315); % axis scale



figure = hs {i};



% ask title name
 answer1 = inputdlg('Enter scatterplot title:'); % ask to get
 R1= answer1;
% title_name (R1) % legend


% title_name = R1;
```

```
title_name = 'Scatter plot magnitude & angle polarity for sfGFP'; % figure title,
avoid special characters, in other case no saved
%title(R1); %to add title





saveas(figure, title_name, 'pdf');



fprintf(1, 'Et voilà!');
```